Stellar Structure

What do these equations mean?

$$\frac{dP}{dr} = -\frac{Gm(r)\rho}{r^2}$$

$$\frac{dm}{dr} = 4\pi r^2 \rho$$

$$\frac{dL}{dr} = 4\pi r^2 \rho q$$

$$\frac{dT}{dr} = \frac{-3\kappa\rho L}{4ac4\pi r^2 T^3}$$

$$\frac{dT}{dr} = \left(\frac{\gamma - 1}{\gamma}\right)\frac{T}{P}\frac{dP}{dr}$$

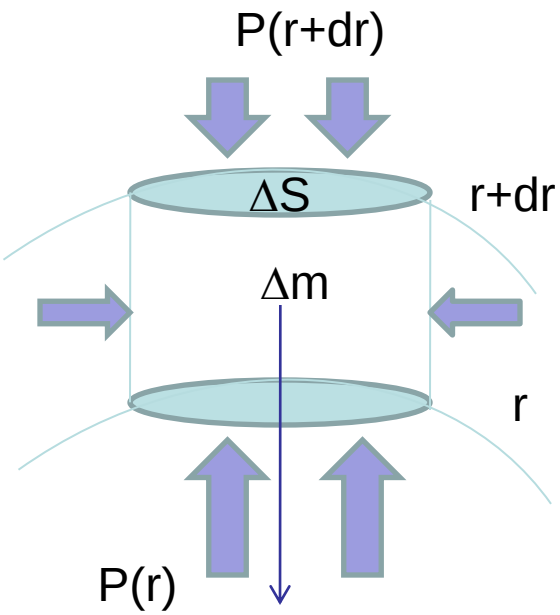

$$P = P(\rho, T, \mu)$$

$$\kappa = \kappa(\rho, T, \mu)$$

$$q = q(\rho, T, \mu)$$

Variables (7): *m*, *ρ*, *T*, *P*, *κ*, *L*, and *q*

Vogt-Russell theorem

In general

$$\ddot{r} = -\frac{Gm}{r^2} - \frac{1}{\rho}\frac{\partial P}{\partial r} = -\frac{Gm}{r^2} - 4\pi r^2 \frac{\partial P}{\partial m}$$

At the center of a star in hydrostatic equilibrium

$$\frac{dP}{dm} = -\frac{Gm}{4\pi r^4}$$

Integrating from the center to the surface

$$P(M) - P(0) = -\int_0^M \frac{Gm\,dm}{4\pi r^4}$$

With the boundary conditions,

$$P(M) \approx 0 \quad P(0) = P_c$$

Thus,

$$P_c = \int_0^M \frac{Gm\,dm}{4\pi r^4} > \int_0^M \frac{Gm\,dm}{4\pi R^4}$$

$$= \frac{GM^2}{8\pi R^4} = 4.4\times 10^{13} \left(\frac{M}{M_\odot}\right)^2 \left(\frac{R_\odot}{R}\right)^4 \ \mathrm{N\ m^{-2}}$$

Stellar Structure

Pressure

Hydrostatic equilibrium

$$\frac{dP}{dr} = -\frac{Gm(r)}{r^2}\rho$$

So $$\frac{P}{R} = \frac{GM}{R^2}\frac{M}{R^3} \rightarrow \boxed{P = \frac{GM^2}{R^4}}$$

Idea gas law

$$P = \frac{\rho}{\mu m_H}kT; \rho = \frac{M}{R^3}$$

So $\boxed{P \sim \frac{M}{R^3}\frac{T}{\mu}}$ and $\boxed{T \sim \frac{\mu GM}{R}}$

This is valid at the star's center,

$$T_* \sim \frac{\mu GM_*}{R_*}$$

Mean molecular weight

$\mu = 1/2$ (H)

$= 4/3$ (He)

$\cong 2$ (metals)

Luminosity

Ohm's law

[flow] ∝ [pressure gradient] / [resistance]

Pressure = [energy] / [volume]

$$
\begin{aligned}
L &\sim 4\pi R^2 \frac{d(\frac{1}{3}aT^4)/dr}{\kappa\rho} \\
&\sim 4\pi R^2 \frac{4}{3}\frac{aT^3}{\kappa\rho}\frac{dT}{dr} \\
&\sim \frac{RT^3}{\kappa\rho}\frac{dT}{dr}
\end{aligned}
$$

Blackbody radiation

Energy density $u = aT^4$

Radiation pressure $P = (1/3)\, u$

For a given structure, $T \sim T_c$, $\frac{dT}{dr} \sim \frac{T_c}{R}$

and $T_c \sim \frac{\mu G M}{R}$

$$\therefore L \sim \frac{R^2 T^4 / R}{\kappa \cdot M/R^3} \sim \frac{R^4 T^4}{\kappa M} \sim \frac{R^4}{\kappa M} \cdot \left(\frac{\mu G M}{R}\right)^4$$

$$\boxed{L \sim \frac{\mu^4 G^4 M^3}{\kappa}}$$

$\kappa = \kappa(\rho, T, \mu)$

- For solar composition, Kramer's opacity applies

$$\boxed{\kappa \sim \rho T^{-3.5}} \qquad 10^4 - 10^6\ K$$

$$\kappa \sim \mu^{-3.5} G^{-3.5} M^{-2.5} R^{0.5}$$

$$\boxed{L \sim \mu^{7.5} G^{7.5} M^{5.5} R^{-0.5}}$$

- For high-mass stars, $T \uparrow$ or $n \downarrow$, Opacity $\Leftarrow e^-$ scattering

$$\kappa \sim \text{const}$$

$$\boxed{L \sim \mu^4 G^4 M^3}$$

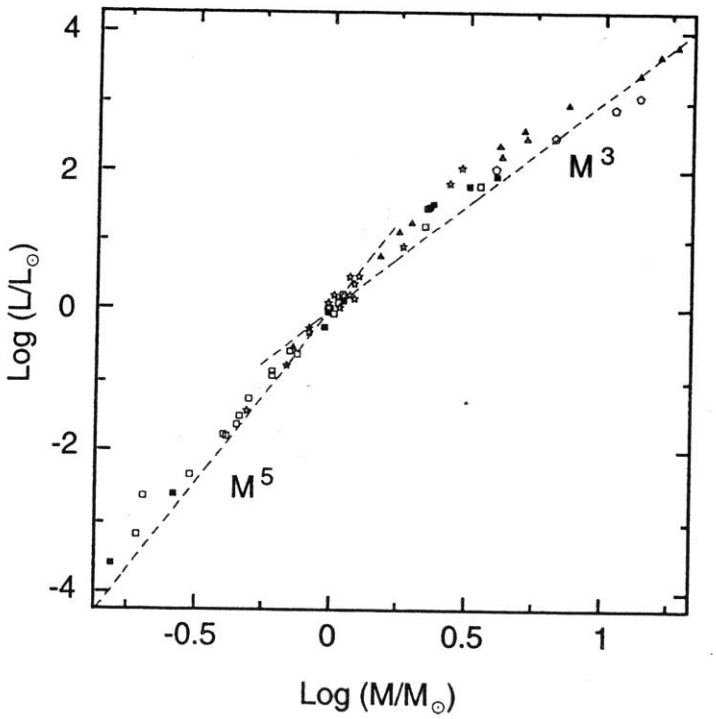

Figure 1.6 The mass–luminosity relation for main-sequence stars. Symbols denote ordinary binary stars (squares); eclipsing variables (triangles); Cepheids (pentagons); double-star statistics (stars).

(a) *Electron scattering* – the scattering of a photon by a free electron, the photon's energy remaining unchanged [known as Compton scattering, or in the nonrelativistic case, more common to stellar interiors, Thomson scattering (after J. J. Thomson)].

(b) *Free-free absorption* – the absorption of a photon by a *free* electron, which makes a transition to a higher energy state by briefly interacting with a nucleus or an ion. The inverse process, leading to the emission of a photon, is known as *bremsstrahlung*.

(c) *Bound-free absorption* – which is another name for photoionization – the removal of an electron from an atom (ion) caused by the absorption of a photon. The inverse process is radiative recombination.

(d) *Bound-bound absorption* – the excitation of an atom that is due to the transition of a (bound) electron to a higher energy state by the absorption of a photon. The atom is then de-excited either spontaneously or by collision with another particle, whereby a photon is emitted.

In stellar interior, $T \uparrow\uparrow$, (a), (b) dominate.

Kramers opacity

Named after the Dutch physicist H. A. Kramers (1894-1952), it is the main source of resistance to the flow of radiation energy in gases of temperature 10^4-10^6, mostly due to transition of free electron. It is the dominant opacity in the interior of stars up to ~ 1 $M_\odot$, and declines as temperature increases $\kappa \propto \rho\, T^{-3.5}$. In stars much more massive, the electron scattering process dominates the opacity, and the Kramers opacity is important only in the surface layers.

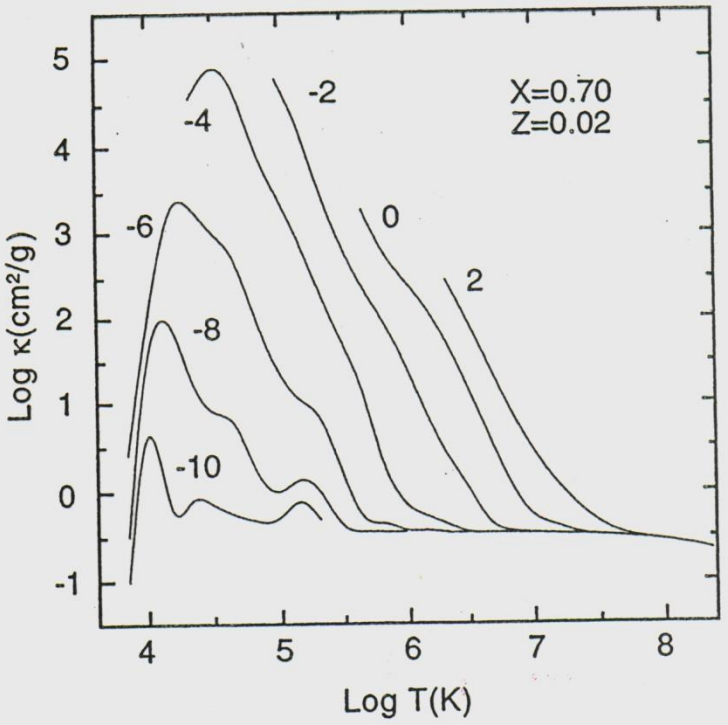

Figure 3.3 Opacity coefficients (in units of $cm^2\ g^{-1}$) for a solar composition as a function of temperature for different density values; the numbers beside each curve are $\log \rho(g\ cm^{-3})$ [data from C. A. Iglesias & F. J. Rogers (1996), *Astrophys. J.*, 464]. 943

$\kappa_{el.scat} = 0.198\,(1 + X_H)\ [cm^2\ g^{-1}]$

Kramer's Opacity $\kappa \sim \frac{\sigma}{m}$ cross section

energy emitted / s / cm^{-3} $\propto$ # of recombination / s / cm^{-3}

(# of recombination) $\propto n_i n_e v_e \sigma \varepsilon$

(複合)

- n_i (ion density) $\propto Z = (1 - X - Y)$
  - H
  - He
- n_e (e^- density) $= \frac{\rho}{m_H} \cdot X \cdot 1 + \frac{\rho}{4 m_H} \cdot Y \cdot 2 + \frac{\rho}{A m_H} \cdot Z \cdot N$

  (N: atomic #)

In general $\frac{N}{A} \approx \frac{1}{2}$

In stars, $Z \ll X$ $\therefore Y \approx 1 - X$

$$n_e = \frac{\rho}{m_H} \left[X + \frac{1}{2}(1 - X) + \cancel{\frac{1}{2} Z}^{\,0} \right]$$

$$= \frac{\rho}{2 m_H} (1 + X)$$

- $v_e \sim \sqrt{\frac{3kT}{m_e}} \sim T^{1/2}$
- σ (collisional) $\propto \frac{1}{v_e^2} \sim T^{-1}$
- $\varepsilon = (E_K$ of $e^-) - ($energy at that level$) \sim T$

Rate of energy absorption = Rate of energy emission

$$\propto \rho (1+X)(1-X-Y) T^{1/2}$$

κ (mass absorption coefficient)

$$\propto \frac{\text{Rate of energy absorption}}{\text{(radiation) energy flow}} \sim T^{1/2} \sim T^{4}$$

$$\boxed{\kappa = \kappa_0 \rho (1+X)(1-X-Y) T^{-3.5}}$$

$\kappa_0 \sim 10^{25}$

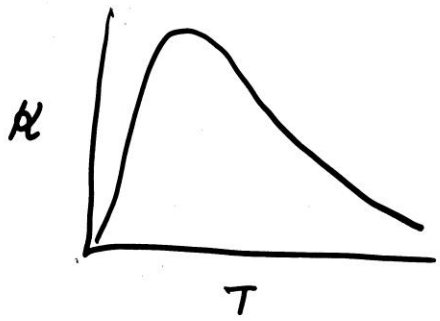

Note: opacity — radiation / convection

protostars: fully convective

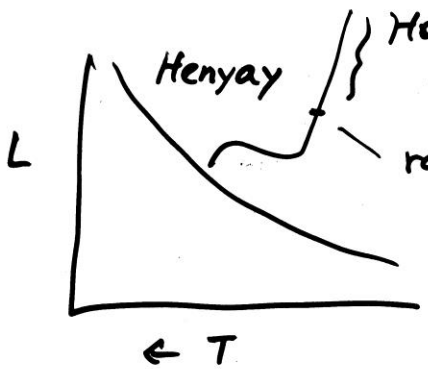

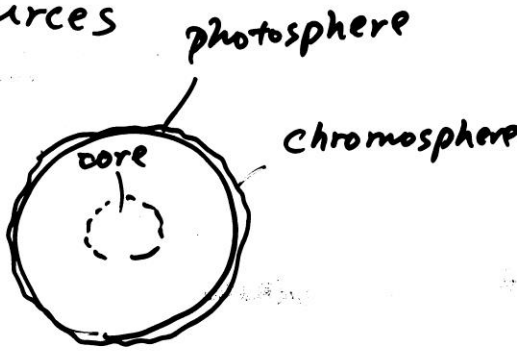

Different temperature, elements (at different excitation and ionization levels)
→ different set of spectral lines

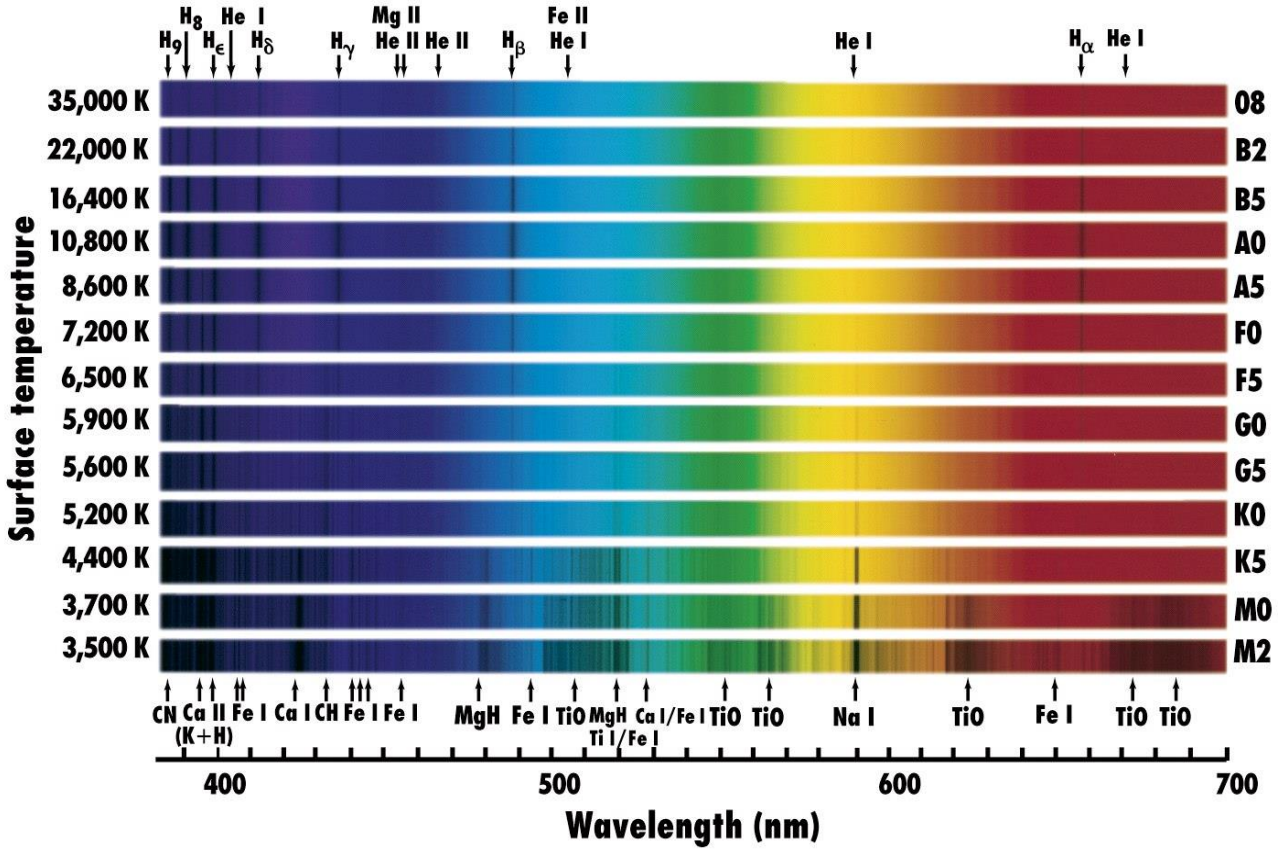

Line ratios → Temperature

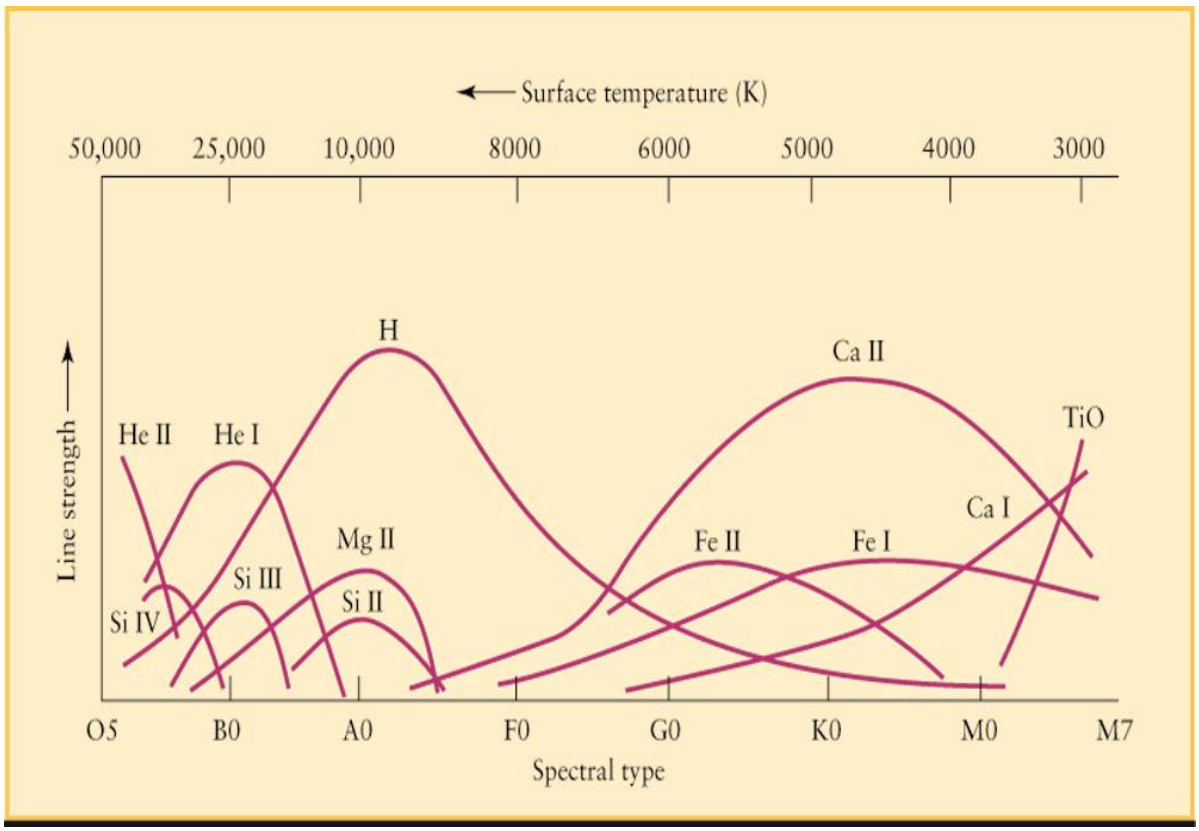

I --- neutral atoms
II --- ionized once
III --- ionized twice
…

Ex. H I, H II, He III, Fe IVX

Hot stars --- peaked at short wavelengths (UV), mainly He lines, some H lines

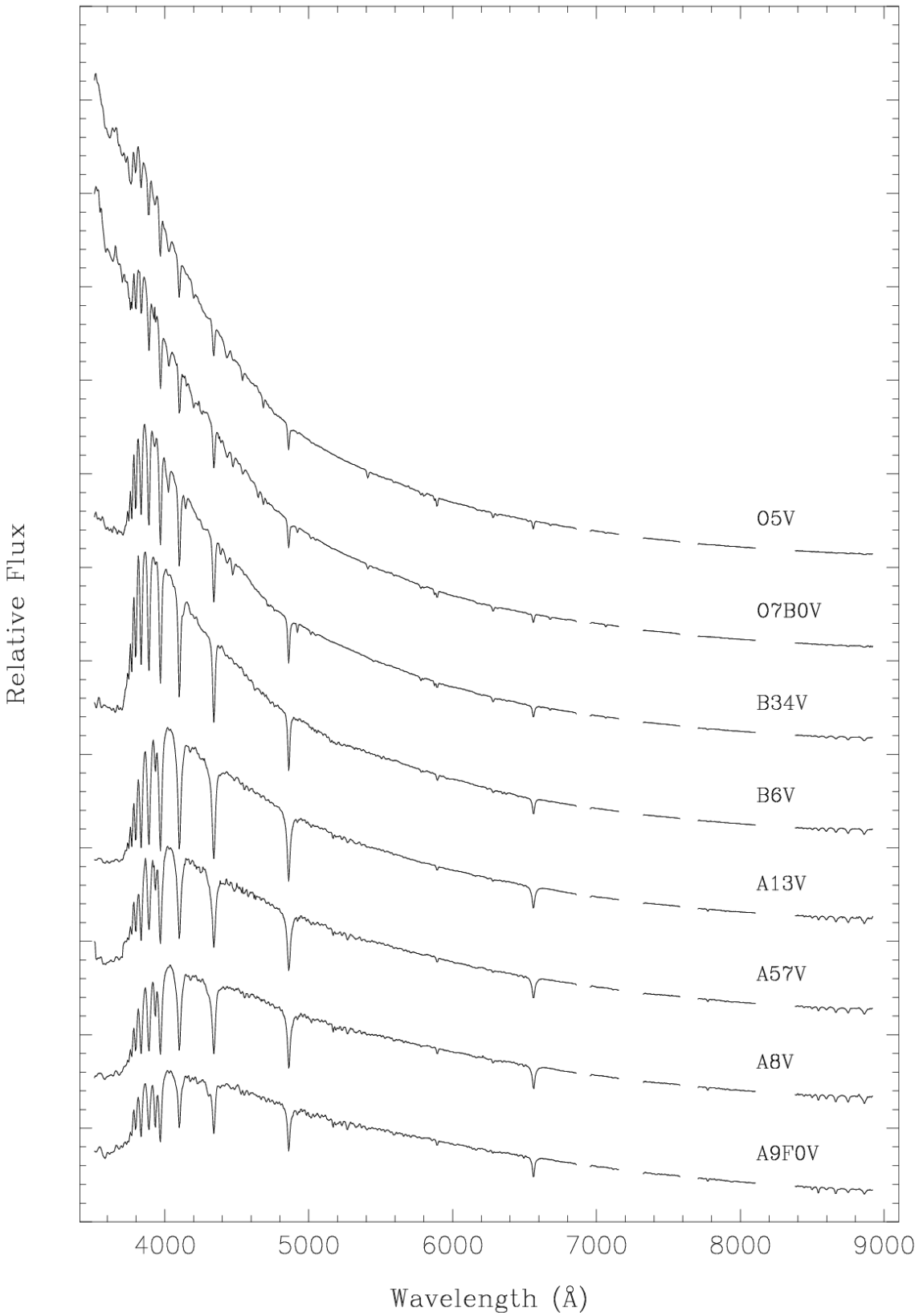

Warm stars --- peaked in the visible wavelengths; H lines prominent

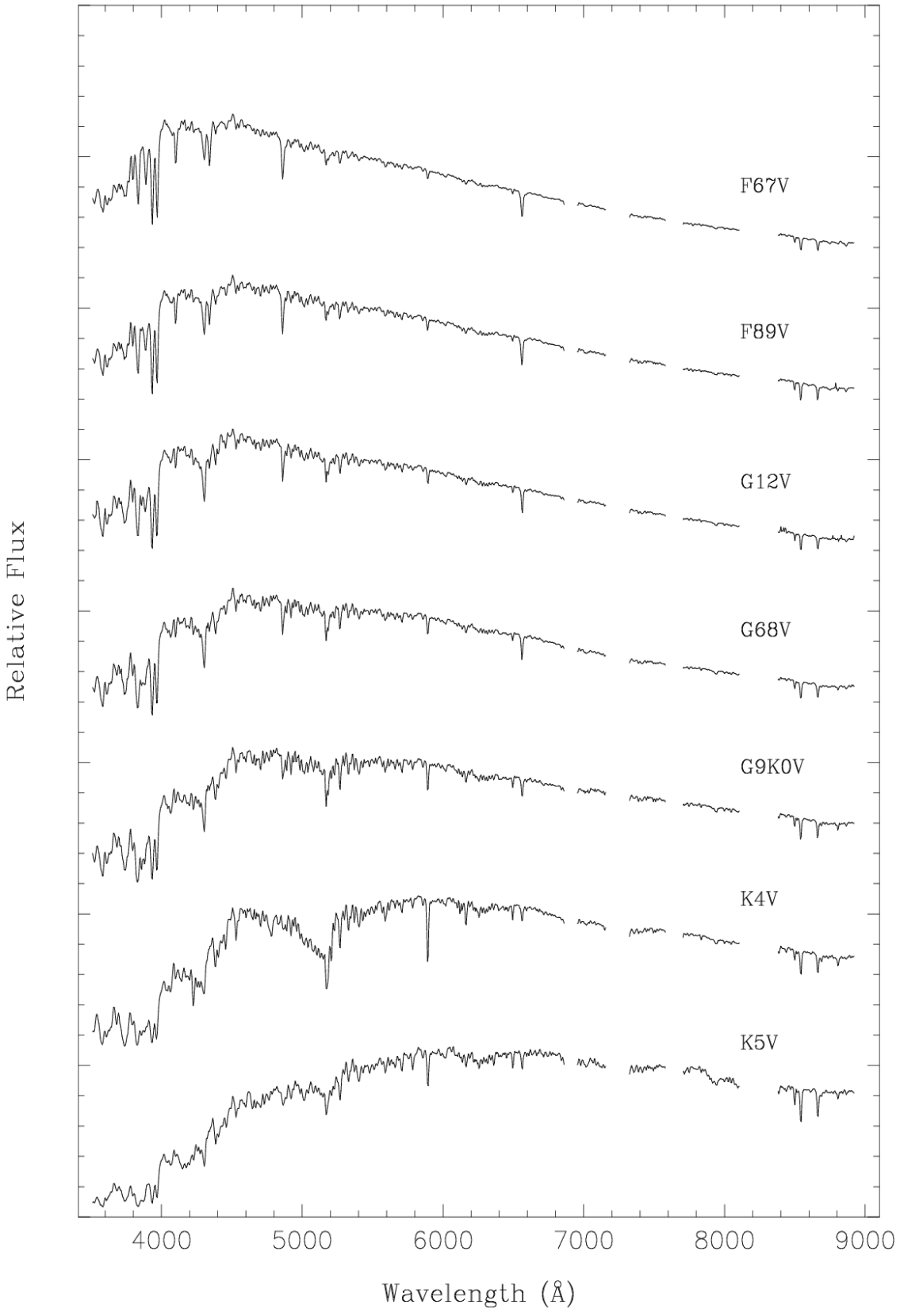

Cool stars --- peaked at long wavelengths (IR); molecular lines/bands

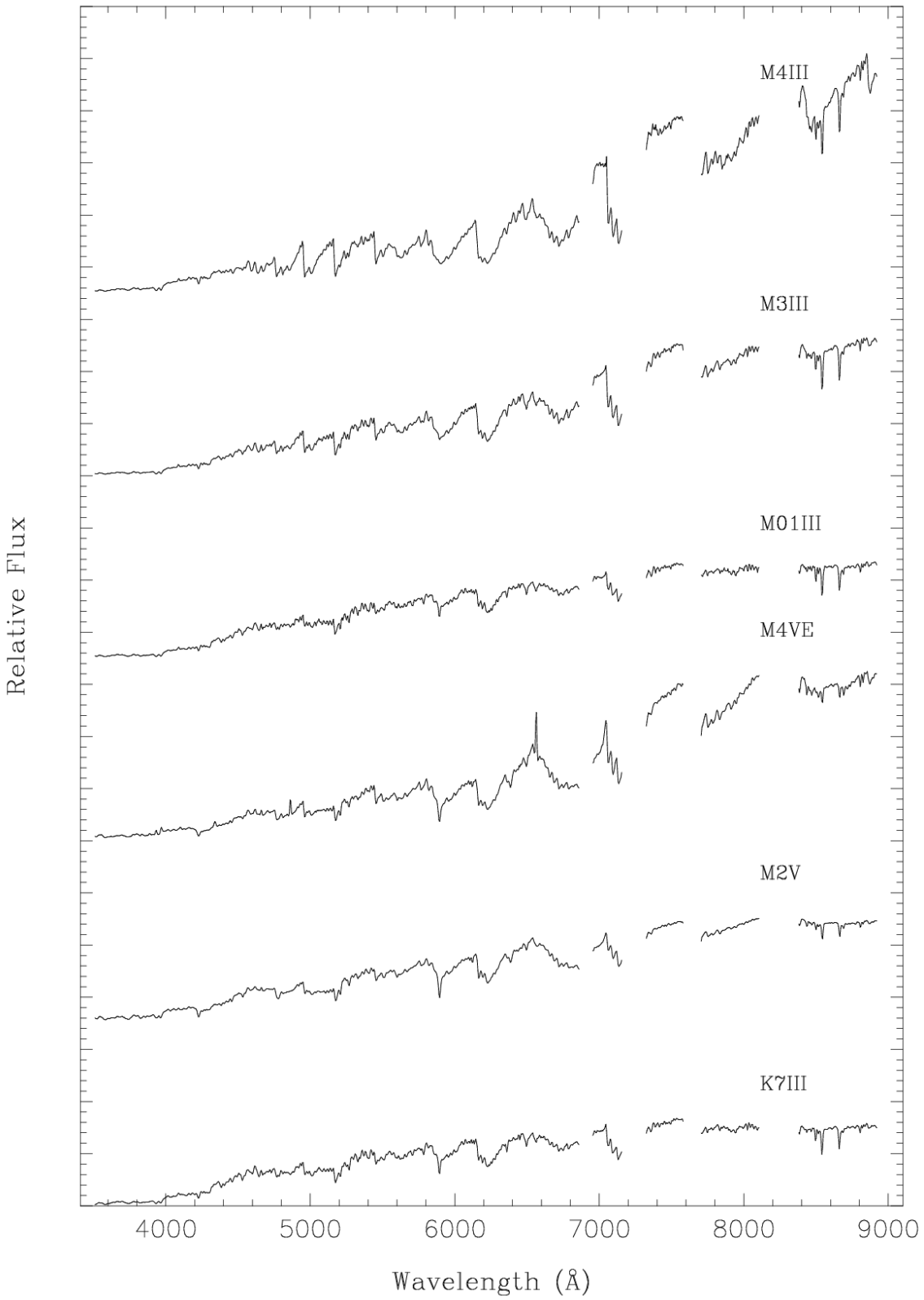

Brown dwarfs

L, T and Y type

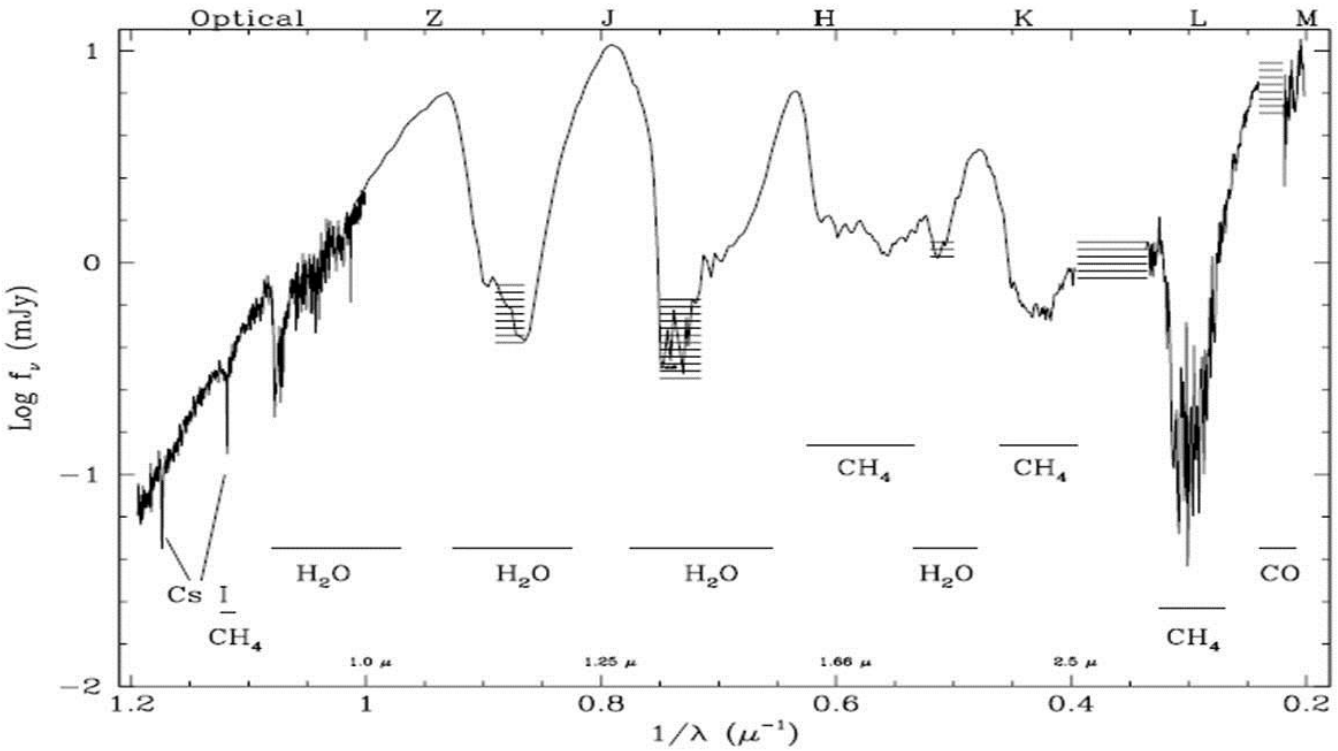

http://farm7.static.flickr.com/6192/6090158853_68cd6f8d42_o.jpg

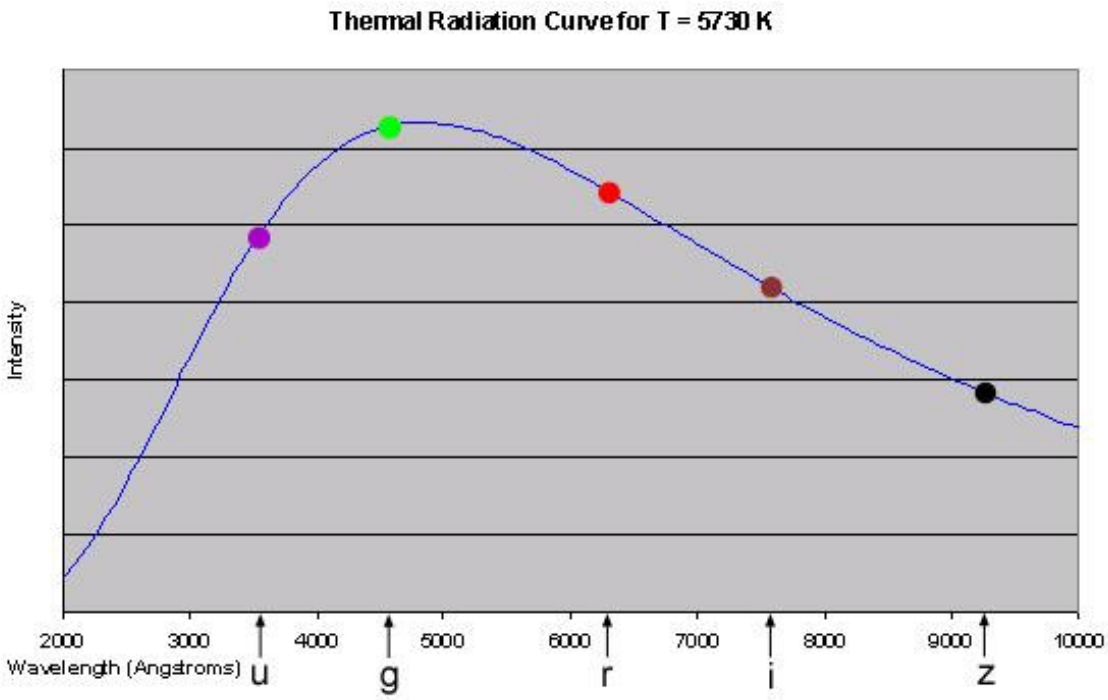

http://cas.sdss.org/dr3/en/proj/advanced/color/images/filters.jpg

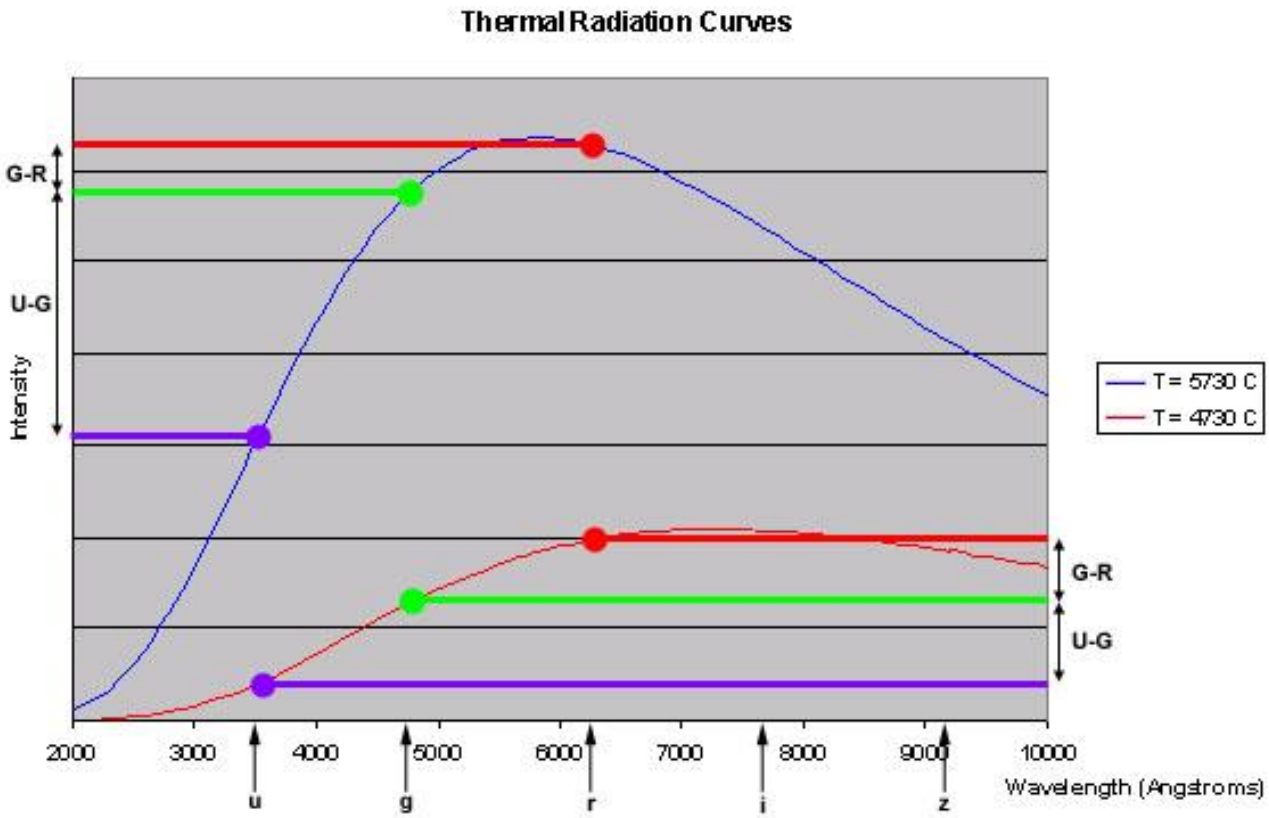

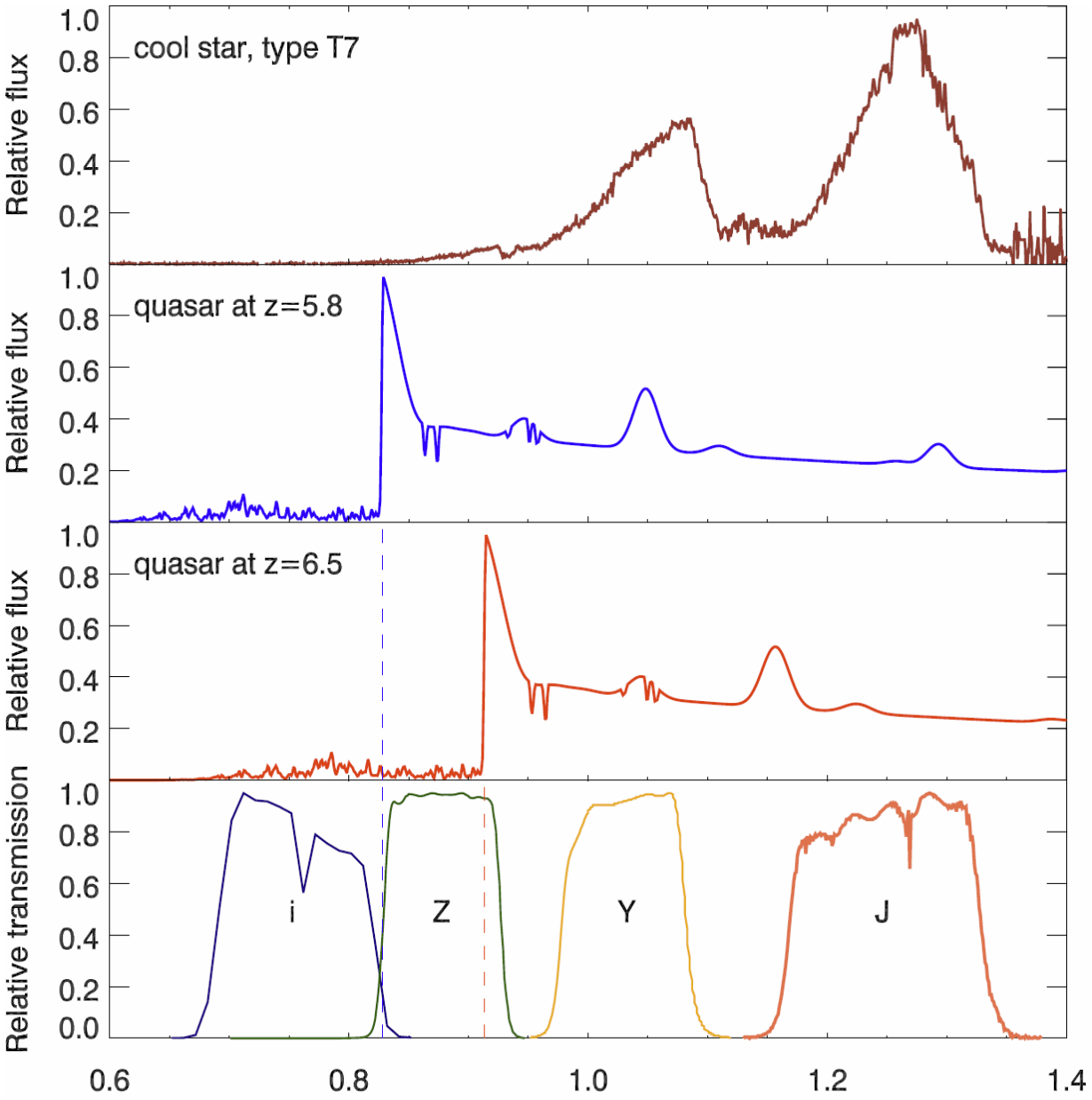
cool star, type T7
quasar at z=5.8
quasar at z=6.5
Relative flux
Relative transmission
i
Z
Y
J
1.0
0.8
0.6
0.4
0.2
0.0
0.6
0.8
1.0
1.2
1.4

One of the SDSS color-color diagrams

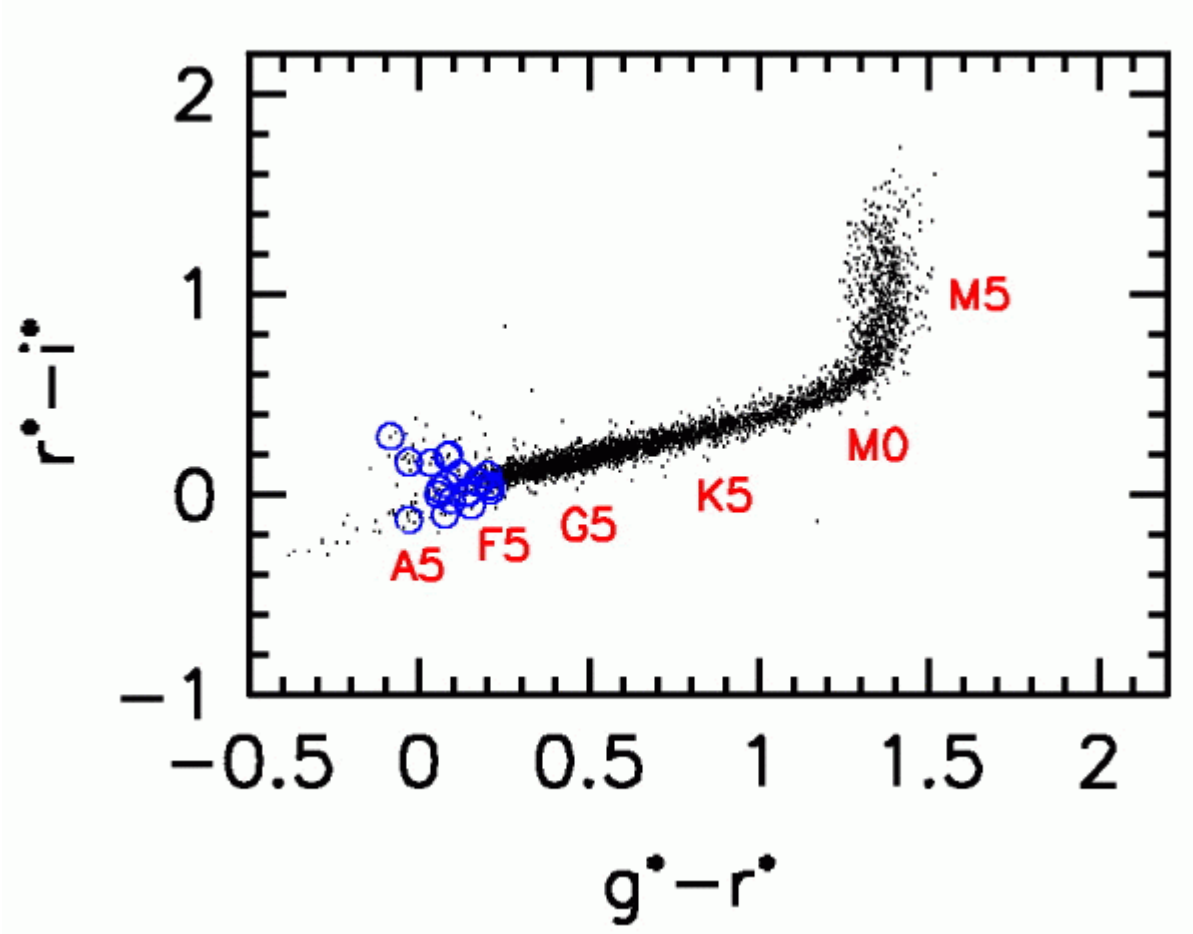

http://spiff.rit.edu/classes/phys440/lectures/color/sdss_color_color_b.gif

Main sequence = a mass sequence defined by hydrogen fusion at the center of a star

Radius does not vary much; but the luminosity does.

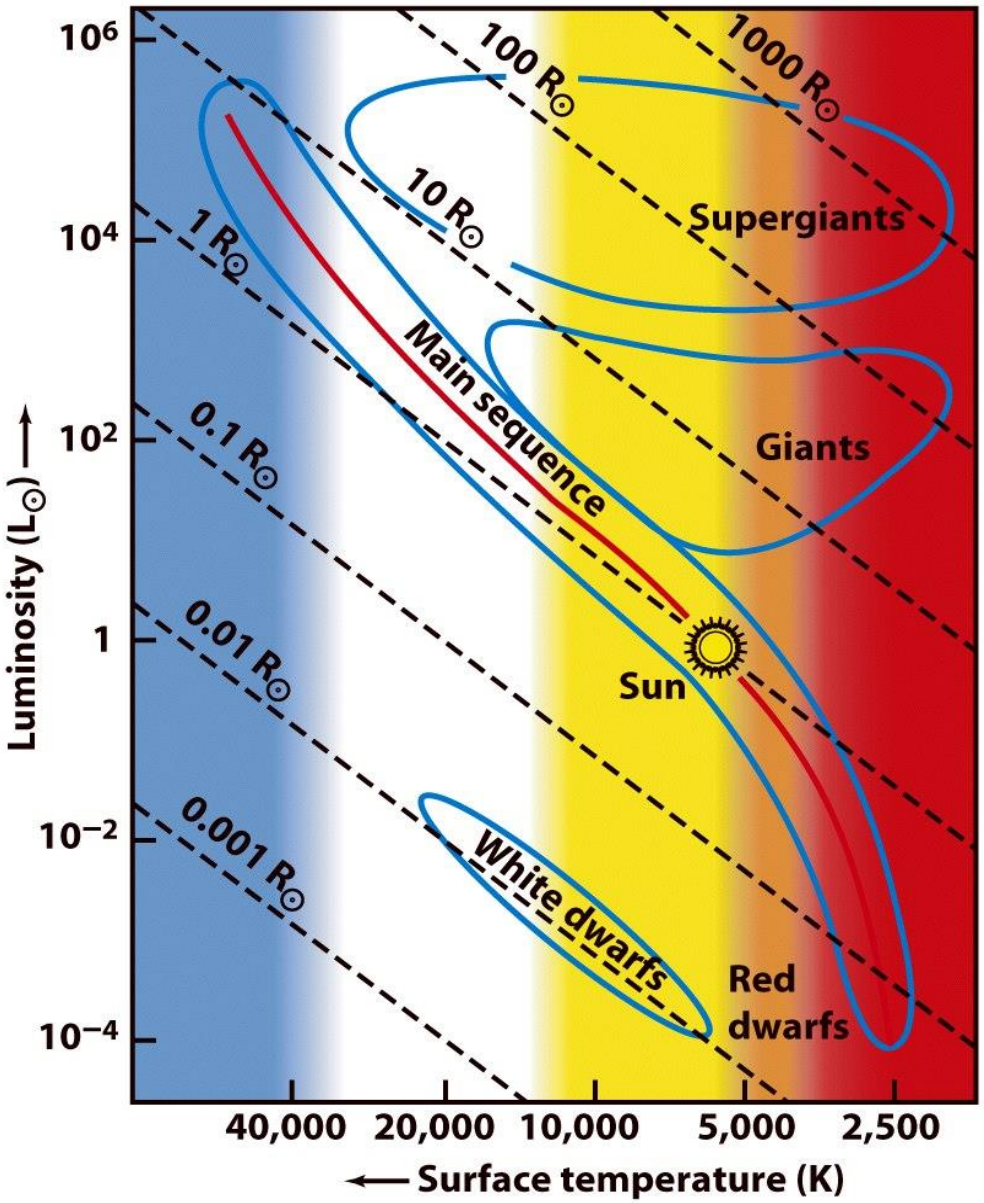

Figure 11-8
Discovering the Universe, Seventh Edition

$$L = (\sigma T^4)(4\pi R^2)$$

$$T_c \sim \frac{\mu M}{R}$$

For a given T_c, $M \xrightarrow{\text{determines}} R$, $M \longrightarrow L$ $\Rightarrow$ L and T_e ($L \propto R^2 T_e^4$)

Main sequence is a run of L and T_e as a function of mass, with T_c nearly constant

why T_c = const

$\because$ H burning at $\sim 10^7$ K

Equation of State

Stability of a star $2E_K + E_p = 0$

$$E_{thermal} = \frac{3}{2} kT = \frac{3}{2}(c_p - c_v) T$$

$$= \frac{3}{2}(\gamma - 1) c_v T$$

$$= \frac{3}{2}(\gamma - 1) U$$

$c_p - c_v = k$

$c_p / c_v \equiv \gamma$

$$E_p = \Omega$$

$\therefore$ $3(\gamma - 1) U + \Omega = 0$

$$E_{total} = U + \Omega = \left[\frac{-1}{3(\gamma-1)} + 1\right]\Omega = \frac{3\gamma - 4}{3(\gamma-1)} \cdot \Omega$$

Note: $\Omega < 0$

$\therefore$ in order to be stable, $E_{total} < 0 \Rightarrow \gamma > \frac{4}{3}$

To determine γ of a star

For an ideal gas $u_i = \frac{1}{2} kT$ per degree of freedom

Equipartition of energy $\Rightarrow$ $u = \sum u_i = \frac{n}{2} kT$, for n dof

Since $c_v = \left(\frac{\partial u}{\partial T}\right)_v = \frac{n}{2} k$

$$\frac{c_p}{c_v} \equiv \gamma = \frac{\frac{n}{2}k + k}{\frac{n}{2}k} = 1 + \frac{2}{n}$$

For an ideal gas, $n = 3$, $\gamma = 5/3$

For a photon gas, $n = 6$ (2 polarization direction
3 propagation direction

$$\gamma = 4/3$$

In general, a star with a mixture of gas and rad.

$$\frac{4}{3} \lesssim \gamma \lesssim \frac{5}{3}$$

$\therefore$ stability criterion is satisfied.

$\gamma \to 4/3$ radiation pressure dominated

$\gamma \to 5/3$ gas pressure dominated

monatomic gas, dof=3 → γ=5/3=1.67

diatomic gas, dof=5, γ=7/5=1.4

Ideal gas

$$P = \frac{N}{V} kT = nkT = \frac{\rho}{\mu m_H} kT$$

$$\therefore \boxed{\frac{dP}{P} = \frac{d\rho}{\rho} + \frac{dT}{T}}$$

$$C_v = \left(\frac{\partial Q}{\partial T}\right)_v \qquad C_p = \left(\frac{\partial Q}{\partial T}\right)_p$$

$$dQ = du + P dV \qquad du = C_v dT$$

$$\left(\frac{\partial Q}{\partial T}\right)_p = C_v + P\left(\frac{\partial V}{\partial T}\right)_p = C_v + Nk$$

$$\boxed{c_p = c_v + nk}$$

$$\gamma = c_p/c_v = \frac{1 + C_v}{C_v} = \frac{1 + n/2}{n/2} = 1 + \frac{2}{n}$$

n: d.o.f.

CONVECTION

How good is energy transportation by radiation?

cf. Schwarzschild

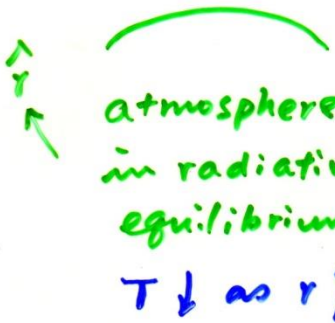

Consider a mass of gas

Rises → expands adiabatically

∴ T ↓

⇒ denser than the surroundings

→ sinks back

∴ Stable in rad. equil.

But if rises, adiabatically cooling, but still warmer than the surroundings

⇒ less denser than surr.

→ keeps rising

⇒ Convection sets in when the adiabatic temp. gradient is smaller than temp. gradient by radiative equil.

i.e., $\left(\frac{dT}{dr}\right)_{ad} < \left(\frac{dT}{dr}\right)_{rad}$

For an adiabatic process, $PV^{\gamma} = constant$

Since $\frac{dP}{dr} = -\rho g$ and $P = \rho k T$

$$dT \cdot \frac{dP}{dr}\frac{1}{P} \propto \frac{1}{T} \cdot dT$$

$$\therefore \frac{dT}{dr} \propto \frac{dT/T}{dP/P} = \frac{d\ln T}{d\ln P}$$

⇒ Criterion for convection equilibrium becomes

$$\left(\frac{d\ln T}{d\ln P}\right)_{ad} < \left(\frac{d\ln T}{d\ln P}\right)_{rad}$$

With the notation ∇ (nabla)

$$\nabla_{ad} < \nabla_{rad}$$

Convection takes place when the temperature gradient is "sufficiently" high (compared with the adiabatic condition) or the pressure gradient is low enough.

Such condition also exists when the gas absorbs a great deal of energy without temperature increase, e.g., with phase change or ionization

➔ when c_V is large or γ is small

How to calculate ∇_{rad} ?

$$\frac{dT}{dr} = -\frac{3}{4ac}\cdot\frac{\kappa\rho}{T^3}\frac{L_r}{4\pi r^2} \qquad \text{but } \frac{dP}{dr} = -g\rho$$

$$\therefore \frac{dT}{dP} \propto \frac{\kappa}{T^3}\frac{L_r}{r^2}$$

$$\nabla_{rad} \equiv \left(\frac{d\ln T}{d\ln P}\right)_{rad} = \frac{dT/T}{dP/P} = \cdots = \frac{3\kappa}{16\pi ac}\frac{P}{T^4}\frac{L_r}{GM_r}$$

>

For an adiabatic process for an ideal gas

$$dQ = c_v dT + P\,d\left(\tfrac{1}{\rho}\right) = c_v dT - \frac{P}{\rho^2}d\rho = 0$$

$$\therefore c_v dT = \frac{P}{\rho^2}d\rho$$

$$c_v\frac{dT}{T} = \frac{P}{\rho T}\cdot\frac{d\rho}{\rho}$$

① $P = nkT \propto \rho T$

$$\frac{dP}{P} = \frac{d\rho}{\rho} + \frac{dT}{T}$$

<=

② $\frac{nR}{\mu} = c_p - c_v$

$$c_v\frac{dT}{T} = (c_p - c_v)\left(\frac{dP}{P} - \frac{dT}{T}\right)$$

③ $\gamma = \frac{c_p}{c_v} = \frac{1+c_v}{c_v}$

$$= \frac{1+n/2}{n/2} = 1+\frac{2}{n}$$

$$\Rightarrow c_p\frac{dT}{T} = (c_p - c_v)\frac{dP}{P}$$

n: d.o.f.

$$\nabla_{ad} \equiv \left(\frac{d\ln T}{d\ln P}\right)_{ad} = \left(\frac{dT/T}{dP/P}\right)_{ad} = 1 - \frac{c_v}{c_p} = 1 - \frac{1}{\gamma}$$

e.g., for monatomic gases, $\gamma = 5/3$ $\quad \nabla_{ad} = 0.4$

Note. $\nabla_{rad} \propto P$

At surface $\nabla_{rad} \to 0$

$\therefore$ $\nabla_{ad} \overset{\text{always}}{>} \nabla_{rad} \Rightarrow$ no convection!

The outermost layers of a star are always in radiative equilibrium.

$\therefore$ Convection occurs either

① large temperature gradient for radiative equilibrium

② small adiabatic temperature gradient

Ionization satisfies both conditions because

① opacity ↑

② e^- receive energy $\Rightarrow$ d.o.f. ↑

$\gamma \downarrow \Rightarrow \nabla_{ad} \downarrow$

$\Rightarrow$ Development of hydrogen convective zones

Likewise, there are 1st and 2nd helium convective zones

For a **very low-mass star**, ionization of H and He leads to a fully convective star ➔ H completely burns off.

For a **sun-like star**, ionization of H and He, and also the large opacity of H^- ions ➔ a convective envelope (outer 30% radius).

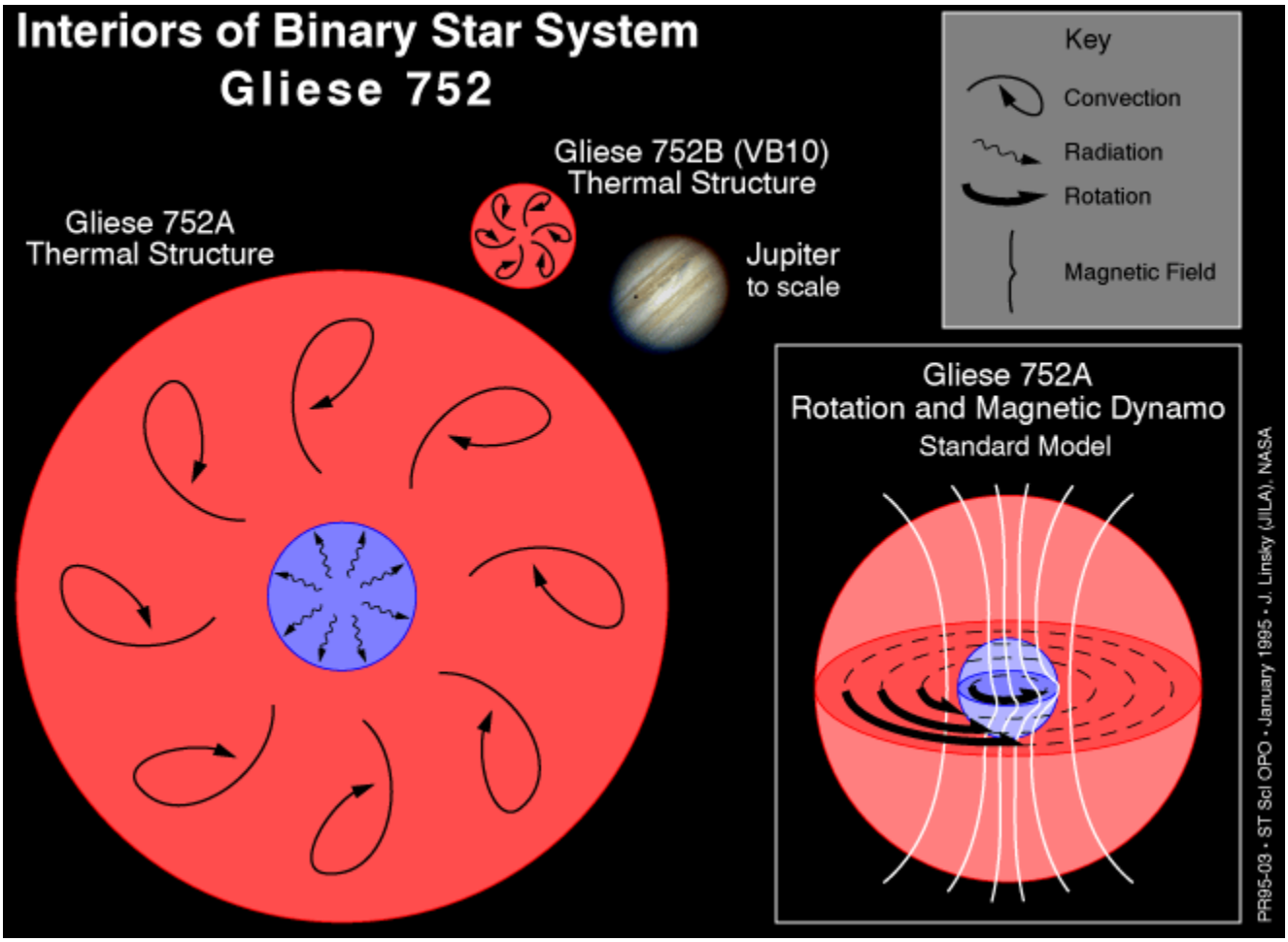

http://hubblesite.org/newscenter/archive/releases/1995/03/image/a/format/large_web/

For a **massive star**, the core produces fierce amount of energy → convective core
➔ a large fraction of material to take part in the thermonuclear reactions

Energy Transport

By radiation

$$\frac{dT}{dr} = \frac{-3}{4ac}\frac{\kappa\rho}{T^3}\frac{L_r}{4\pi r^2}$$

L_r: luminosity

κ: opacity

(electron scattering, b-f, f-f, H^-)

If temperature gradient is too large, then

By convection (unstable to convection; convective instability)

criterion $\boxed{\nabla > \nabla_{ad}}$

$$\nabla \equiv \frac{d\ln T}{d\ln P} \qquad \nabla_{ad} \equiv \left(\frac{d\ln T}{d\ln P}\right)_{ad} = \frac{\gamma-1}{\gamma}$$

γ: adiabatic index

Note For radiative transport

$$\nabla_{rad} \equiv \left(\frac{d\ln T}{d\ln P}\right)_{rad} = \frac{3\kappa}{16\pi a c}\frac{P}{T^4}\left(\frac{L_r}{GM_r}\right)$$

In case of convection

$$\nabla \equiv \frac{d\ln T}{d\ln P} = \frac{P}{T}\frac{dT/dr}{dP/dr} \overset{\text{hydrostatic equil}}{=} -\frac{r^2}{GM_r}\left(\frac{P}{\rho T}\right)\frac{dT}{dr} \simeq \nabla_{ad}$$

$$\therefore \frac{dT}{dr} = -\nabla_{ad}\frac{GM_r}{r^2}\frac{\rho T}{P} = -\frac{\gamma-1}{\gamma}\frac{GM_r}{r^2}\frac{\rho T}{P}$$

If a mol. cloud, Jeans criterion is met

⇒ cloud collapse ⇒ fragmentation

If each fragment, Jeans criterion

⇒ fragment collapses individually ⇒ star cluster

→ a protostar (observationally, Bok globules in opt.
mol. cores in mm)

$D \sim 0.01$ pc

$t \sim 10^6 - 10^7$ yrs

$T \sim 10$ K

$n \sim 10^6 - 10^7$ cm^{-3}

2nd stage

→ free fall

$D \sim 0.001$ pc

$t \sim 10^4 - 10^5$ yrs

$T \sim 10$ K —— isothermal ⇐ line cooling (molecular)

$n \sim 10^{12}$ cm^{-3}

Now, at this density, material becomes opaque to the mol. line emission

⇒ collapse → heating the protostar (T ↑)

⇒ slow down the collapse

Note : inside-out collapse $L_{acc} = GM_{core}\dot{M}/R_{core}$ ($\dot{M}$: mass inflow rate)

3rd stage object is optically thick

$T_{center} \sim 1500 - 2000\ K$

$n_{center} \sim 10^{20}\ cm^{-3}$

$D_{core} \lesssim 1\ AU$

At $T \sim 2000\ K$, H_2 start to dissociate

(requiring $2 \times 10^{12}\ erg\ g^{-1}$)

$\Rightarrow$ isothermal process ($T \sim 2000\ K$)

For $1\ M_\odot$ star, 4×10^{45} erg needed

Once H_2 all dissociated, T ↑ again

At $T \sim 6000\ K$, H starts to ionize

$\Rightarrow$ another isothermal contraction

Hayashi Track

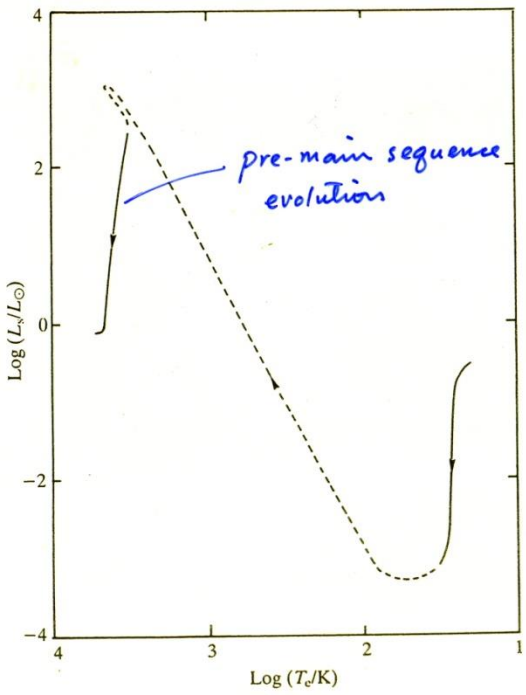

Fig. 53. The complete pre-main-sequence evolution of a star of solar mass.

When a protostar reaches hydrostatic equilibrium, there is a minimum effective temperature (~4000 K) cooler than which (the **Hayashi boundary**) a stable configuration is not possible (Chushiro Hayashi 1961).

A protostar

- contracts on the Kevin-Helmholtz timescale
- is cool and highly opaque → fully convective → homogenizes the composition

Stars < 0.5 $M_\odot$ remain on the Hayashi track throughout the entire PMS phase.

Convective instability

Convection layer
⇒ R_* ↓ than pure radiative case

⇒ A radius maximum for a given mass and luminosity

⇒ A temperature min

$T < T_{min}$
convectively unstable

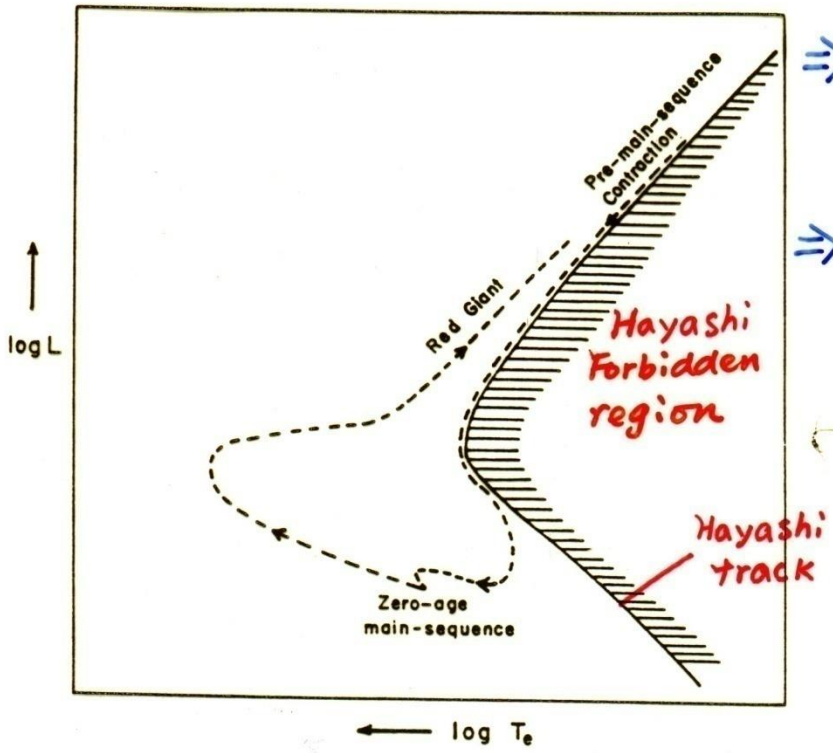

Figure 1. Schematic evolutionary path of a star of 0.8 $M_\odot$.

(Hayashi 1966)
Chushiro H.
林忠四郎

convection occurs when

$$\nabla_{rad} > \nabla_{ad}$$

∴ convection if
(1) ∇_{rad} is large, or
(2) ∇_{ad} is small

$$\nabla_{rad} = \frac{dT}{dr} \sim \frac{L_r}{r^2} \frac{\kappa\rho}{\sigma T^3}$$

$$\nabla_{ad} = 1 - \frac{1}{\gamma} \quad (\gamma = c_p/c_v)$$

∴ ∇_{ad} v. small ⇔ c_v v. large

e.g. H_2 dissociation
H ionization, $T \sim 6000$K
HeI ionization, $T \sim 20{,}000$K
HeII ionization, $T \sim 50{,}000$K

Chushiro HAYASHI 1920-2010

Chushiro Hayashi

From Wikipedia, the free encyclopedia

Chushiro Hayashi (林 忠四郎 *Hayashi Chūshirō*, July 25, 1920 – February 28, 2010) was a Japanese astrophysicist. Hayashi tracks on the Hertzsprung-Russell diagram are named after him.

Chūshirō Hayashi	
Born	July 25, 1920
Died	February 28, 2010 (aged 89) Kyoto, Japan
Nationality	Japan
Fields	astrophysics
Institutions	Kyoto University
Alma mater	University of Tokyo
Influences	Hideki Yukawa
Notable awards	Eddington Medal in 1970 Kyoto Prize in 1995 Bruce Medal in 2004

He earned his B.Sc in physics at the Imperial University of Tokyo in 1942. He then worked as a research associate under Hideki Yukawa at Kyoto University. He made additions to the big bang nucleosynthesis model that built upon the work of the classic Alpher-Bethe-Gamow paper.[1] Probably his most famous work was the astrophysical calculations that led to the Hayashi tracks of star formation,[2] and the Hayashi limit that puts a limit on star radius. He was also involved in the early study of Brown dwarfs, some of the smallest stars formed.[3] He retired in 1984.

He won the Eddington Medal in 1970, the Kyoto Prize in 1995, and the Bruce Medal in 2004.

Chushiro Hayashi died from pneumonia at a Kyoto hospital on February 28, 2010.[4][5]

References

1. ^ Hayashi, C. (1961). "Proton-neutron concentration ratio in the expanding Universe at the stages preceding the formation of the elements". *Progress of Theoretical Physics (Japan)* **5** (2): 224–235. doi:10.1143/PTP.5.224 (http://dx.doi.org/10.1143%2FPTP.5.224) .
2. ^ Hayashi, C. (1961). "Stellar evolution in early phases of gravitational contraction". *Publ. Astron. Soc. Jap.* **13**: 450–452.
3. ^ Hayashi, C.; T. Nakano (1963). "Evolution of Stars of Small Masses in the Pre-Main-Sequence Stages". *Progress of Theoretical Physics* **30** (4): 460–474. doi:10.1143/PTP.30.460 (http://dx.doi.org/10.1143%2FPTP.30.460) .
4. ^ Sugimoto, D. (2010). "Chushiro Hayashi 1920–2010". *Astronomy & Geophysics* **51** (3): 3.36. doi:10.1111/j.1468-4004.2010.51336.x (http://dx.doi.org/10.1111%2Fj.1468-4004.2010.51336.x) .
5. ^ "Award-winning Japanese astrophysicist Hayashi dies at 89" (http://www.japantoday.com/category/national/view/award-winning-japanese-astrophysicist-hayashi-dies-at-89) . Kyodo News. March 1, 2010. Retrieved March 1, 2010.

Henyey track

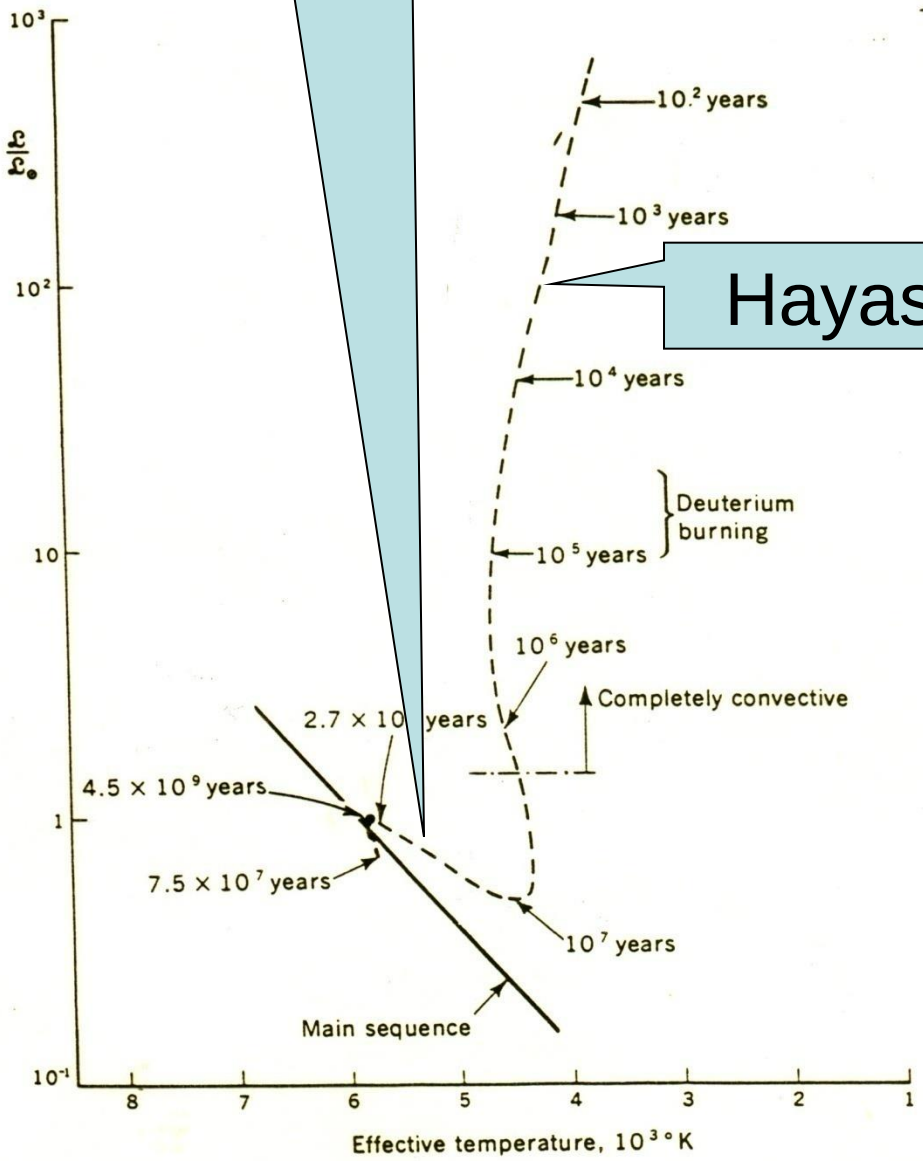

Hayashi track

Fig. 5-1 The path on the H-R diagram of the contraction of the sun to the main sequence. The interior has become sufficiently hot to burn deuterium after about 10^5 years. The contraction ceases near the main sequence when the core has become hot enough to replenish the solar luminosity with the thermonuclear power generated by the fusion of hydrogen into helium. [*After D. Ezer and A. G. W. Cameron, The Contraction Phase of Stellar Evolution, in R. F. Stein and A. G. W. Cameron (eds.), "Stellar Evolution," Plenum Press, New York,* 1966.]

Check out
http://www.peripatus.gen.nz/Astronomy/HerRusDia.html
for a good summary

Astron. & Astrophys. 30, 423–430 (1974)

The Evolution of a Massive Protostar

I. Appenzeller and W. Tscharnuter
Universitäts-Sternwarte Göttingen

Summary. The hydrodynamic evolution of a massive protostar has been calculated starting from a homogeneous gas and dust cloud of 60 $M_\odot$ and an initial density of 10^{-19} g cm^{-3}. Initially the collapsing gas cloud evolved similar to protostar models of lower mass. About 3.6×10^5 years after the beginning of the collapse a small hydrostatic core was formed. About 2×10^4 years later hydrogen burning started in the center of the hydrostatic core. After another 2.5×10^4 years the collapse of the envelope was stopped and reversed by the heat flow from the interior and the entire envelope was blown off, leaving behind an almost normal main-sequence star of about 17 $M_\odot$. During most of the core's evolution the central region of the protostar would have looked like a cool but luminous infrared point source to an outside observer.

Key words: star formation – stellar evolution – infrared sources

Read this paper!

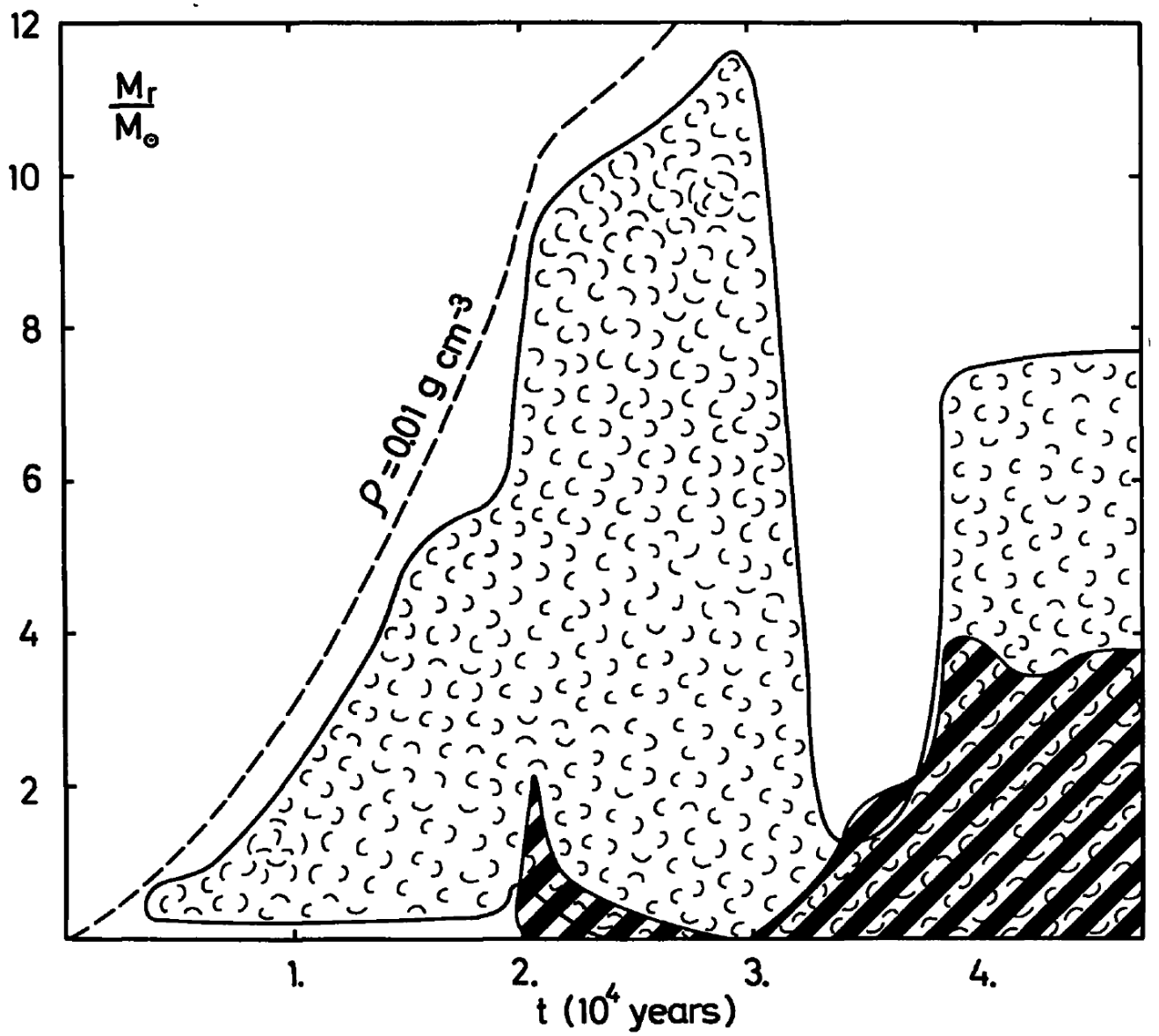

Fig. 5. The variation of the internal structure of the evolving hydrostatic core. The abscissa gives the time since the formation of the (final) hydrostatic core. ($t=0$ corresponds to an age of the protostar of 361473 years.) "Cloudy" regions represent convection. Cross-hatched regions represent nuclear energy generation at a rate exceeding 10^3 erg g^{-1} s^{-1}. The approximate extent of the hydrostatic core is indicated by the line $\varrho = 0.01$ g cm^{-1}

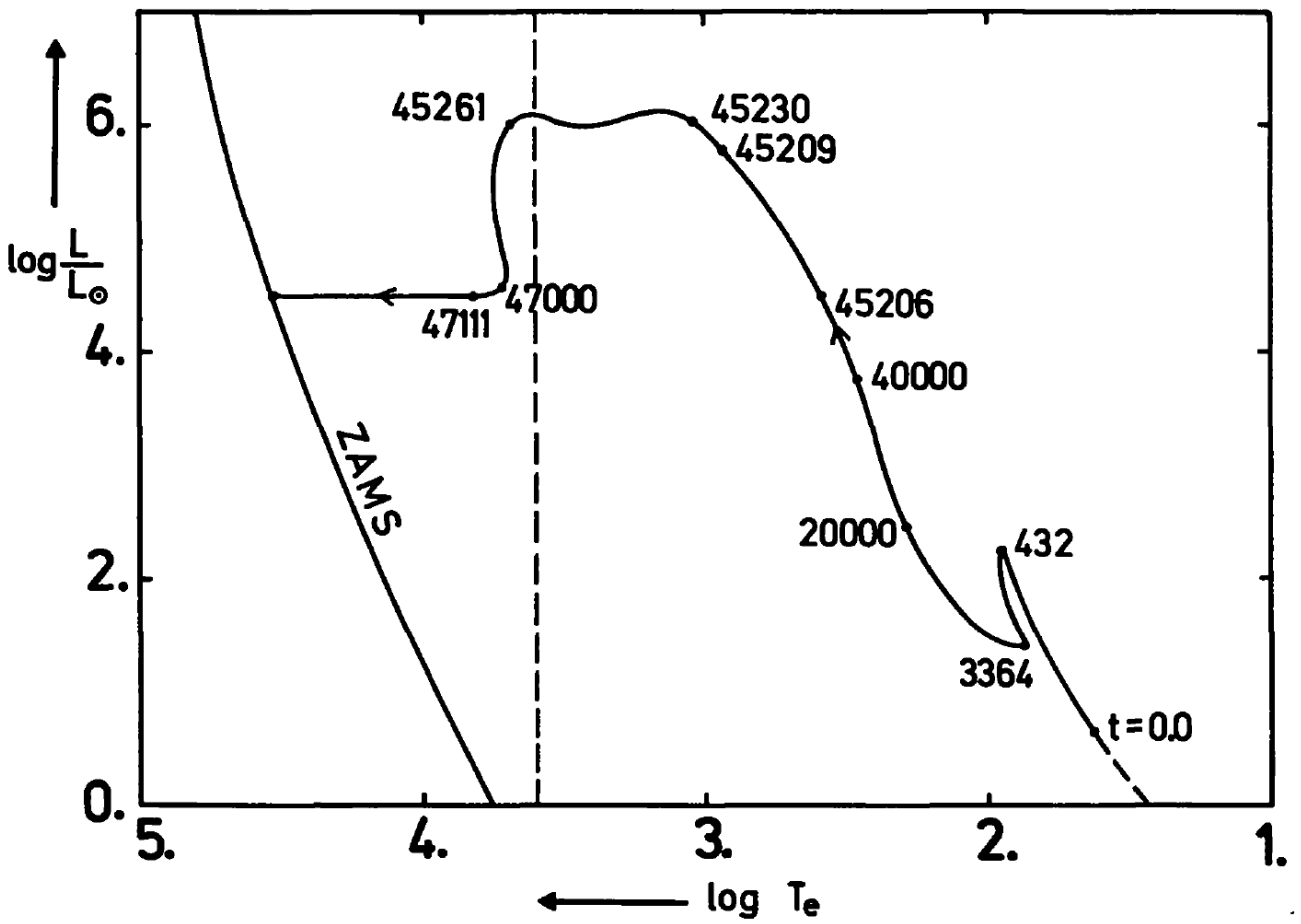

Fig. 6. Approximate evolutionary path of the optically thick central region of the 60 $M_\odot$ protostar in an infrared HR diagram. The numbers indicate the time t since the formation of the final hydrostatic core (c.f. Fig. 5). For comparison we also included the position of the zero-age main-sequence (ZAMS). The broken line gives the approximate lower limit of the effective temperature of hydrostatic configurations (Hayashi *et al.*, 1962)

Astron. & Astrophys. 40, 397—399 (1975)

On the Luminosity of Spherical Protostars

I. Appenzeller*
Universitäts-Sternwarte Göttingen

W. Tscharnuter
Universitäts-Sternwarte Göttingen and Max-Planck-Institut für Physik und Astrophysik München

Summary. Hydrodynamic model computations have been carried out for a spherically symmetric $1\,M_\odot$ protostar. Compared to similar computations by Larson (1969) we used a different treatment of the accretion shock front. Our computations basically confirm Larsons results and show that Larson's disputed shock jump conditions have little influence on the protostellar models.

Key words: star formation — protostars — YY Orionis stars

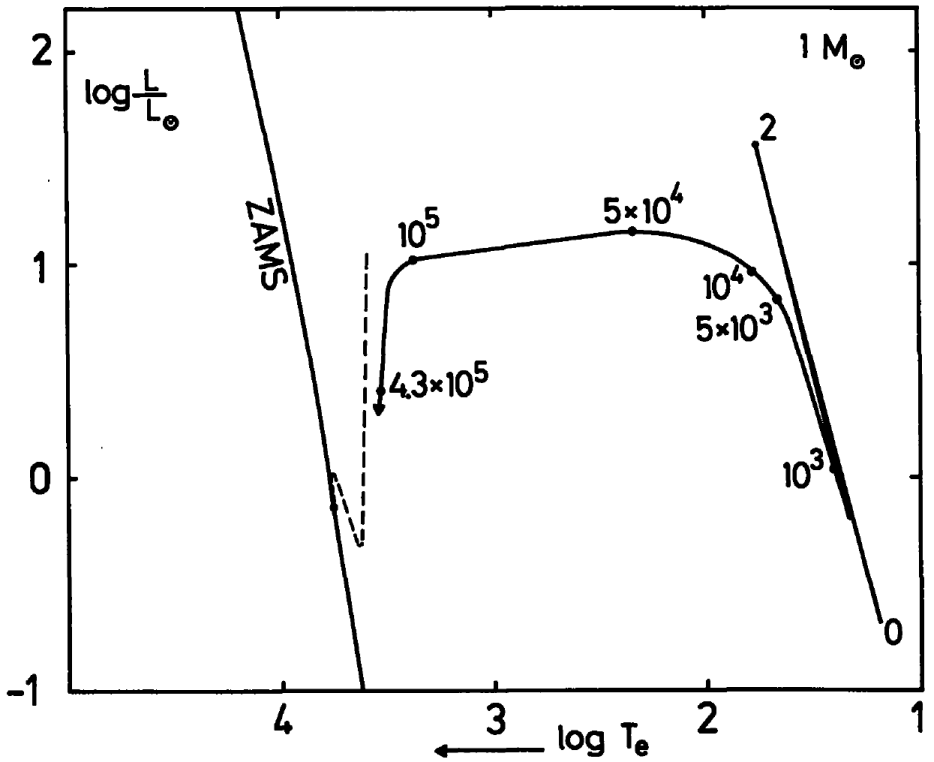

Fig. 1. Evolutionary path of a 1 $M_\odot$ protostar in an infrared HR diagram (solid line). The numbers indicate the time (in years) since the formation of the (final) hydrostatic core. For comparison, the evolutionary path of a conventional fully hydrostatic 1 $M_\odot$ pre-main sequence star is also included (broken line)

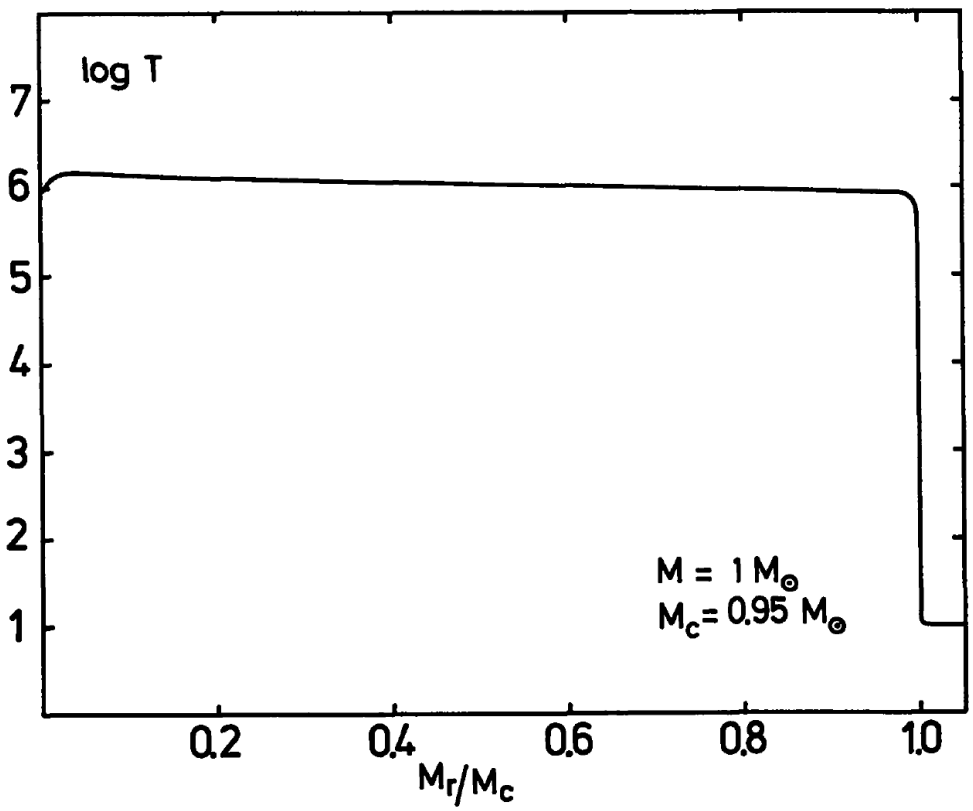

Fig. 2. Temperature distribution in the hydrostatic core of a 1 $M_\odot$ protostellar model after 95% of the total mass has accumulated in the core

Received August 18, 1964, revised November 25, 1964

1965ApJ...141..993

ABSTRACT

The manner in which nuclear reactions replace gravitational contraction as the major source of stellar luminosity is investigated for model stars of population I composition in the mass range $0.5 < M/M_{\odot} < 15\ 0$. By following in detail the depletion of C^{12} from high initial values down to values corresponding to equilibrium with N^{14} in the C-N cycle, the approach to the main sequence in the Hertzsprung-Russell diagram and the time to reach the main sequence, for stars with $M \geq 1.25\ M_{\odot}$, are found to differ significantly from data reported previously.

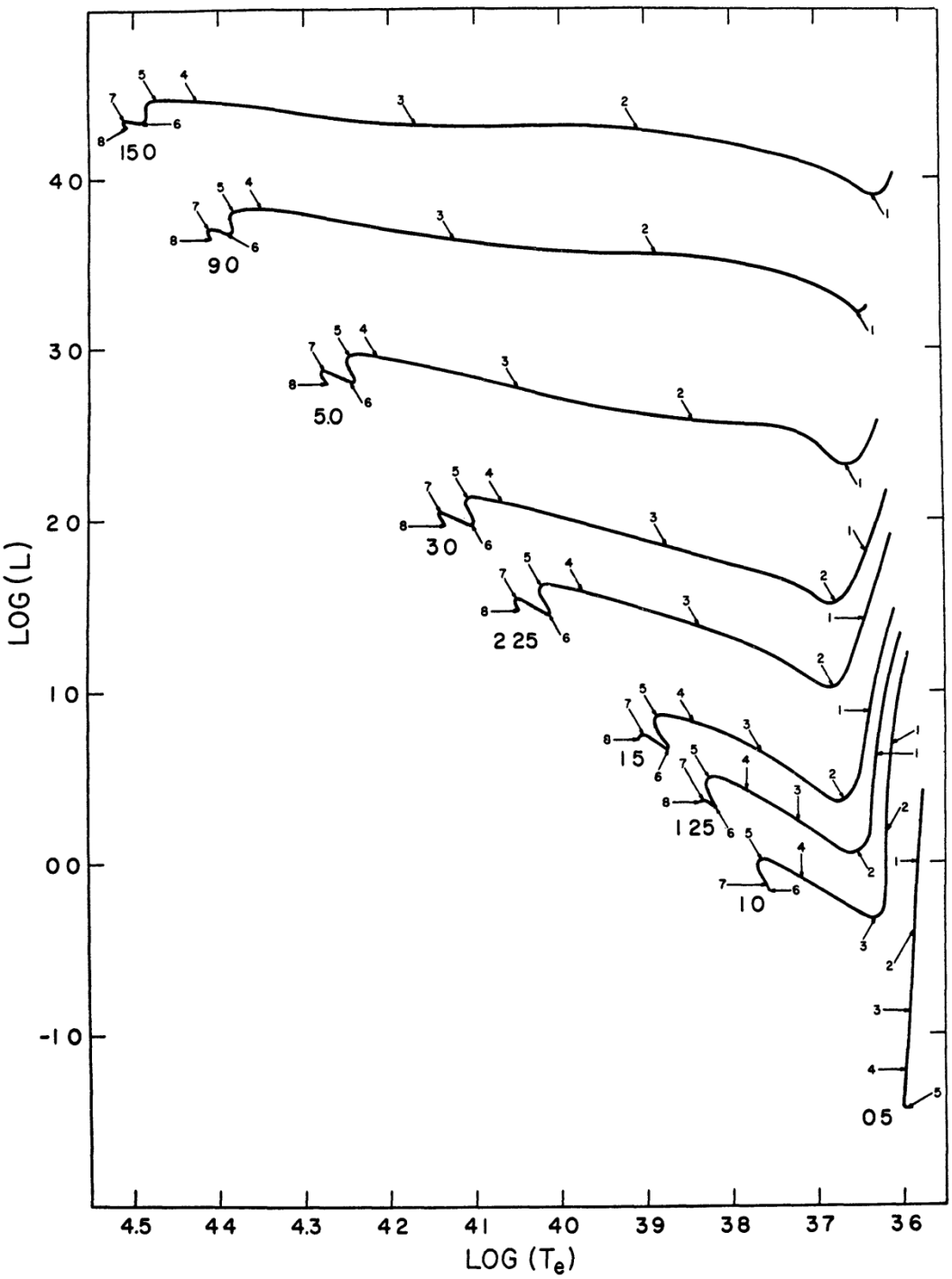

FIG. 17.—Paths in the Hertzsprung-Russell diagram for models of mass $(M/M_{\odot}) = 0.5$, 1.0, 1.25, 1.5, 2.25, 3 0, 5.0, 9.0, and 15.0. Units of luminosity and surface temperature are the same as those in Fig. 1

Chemical abundances (“metals”) are important in determination of stellar structure.

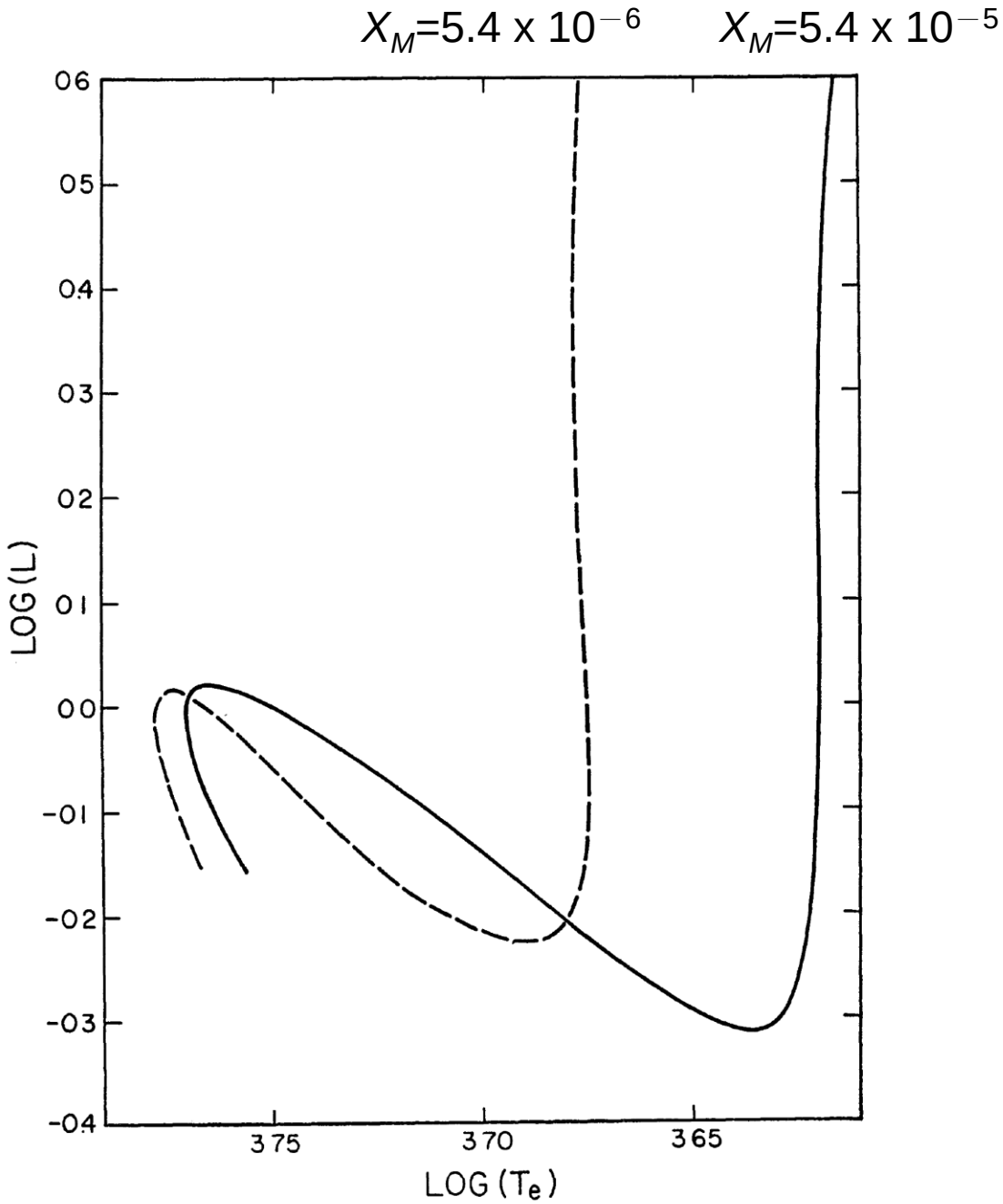

FIG. 1.—Paths in the theoretical Hertzsprung-Russell diagram for $M = M\odot$. Luminosity in units of $L\odot = 3.86 \times 10^{33}$ erg/sec and surface temperature T_e in units of ° K. Solid curve constructed using a mass fraction of metals with 7.5-eV ionization potential, $X_M = 5.4 \times 10^{-5}$. Dashed curve constructed with $X_M = 5.4 \times 10^{-6}$.

17 February 1967, Volume 155, Number 3764 SCIENCE

Stellar Evolution: Comparison of Theory with Observation

Comparison of stellar models with the observations tells us about the interior structure of real stars.

Icko Iben, Jr.

How a star forms and how a star of a given initial mass may approach its end are still unanswered questions. On the other hand, our understanding of those nuclear-burning phases in which a star spends most of its active, luminous life is relatively secure. Puzzles still remain, and the theoretical structure is far from complete, but, on the whole, comparison between the observations and theoretical models of evolving stars engenders confidence. It is my primary purpose here to elaborate my reasons for maintaining this confidence and, at the same time, to point out a puzzle which remains and, by remaining, helps make stellar evolution an active and exciting field.

Evolution of a Typical Metal-Rich Star

At the surface of most of the stars in our galaxy, hydrogen and helium are much more abundant than all of the other elements put together. For example, for every gram of hydrogen and helium near the surface of the sun, there are only a few hundredths of a gram of elements heavier than helium. In the great majority of stars in our galaxy, the surface abundances of the heavier elements are considerably smaller than they are at the surface of the sun. We therefore call the sun a metal-rich star, despite the fact that metals in the sun are much less abundant than hydrogen and helium. In the total makeup of our galaxy, metal-poor stars considerably outnumber metal-rich stars. However, many of the brightest stars in the disk of our galaxy and in the neighborhood of our sun are metal-rich. In particular, this is true of many of the brightest stars in the familiar constellations such as Orion and Taurus. If for no other reason, this makes metal-rich stars, for me, highly interesting subjects of study.

For definiteness, I shall focus on a star of mass five times that of the sun (5 $M_\odot$) (*1*) and suppose that the abundances of the elements in the initial model are roughly similar to those near the surface of the sun. To be specific, out of every gram of stellar matter, I shall suppose that hydrogen (H^1), helium (He^4), carbon (C^{12}), nitrogen (N^{14}), and oxygen (O^{16}) contribute a mass of 0.71, 0.27, 3.6×10^{-3}, 1.2×10^{-3}, and 1.1×10^{-2} gram, respectively. I shall lump the remainder of the elements together rather indiscriminately to complete the specification of initial composition.

For the purpose of checking the adequacy of the theoretical models, the most important result of an evolutionary calculation is a time-dependent relationship between observable quantities. The changing relationship between the surface temperature and luminosity of the 5-$M_\odot$ model star is most conveniently described by means of a path in the so-called Hertzsprung-Russell diagram, as shown in Fig. 1. In this diagram, the logarithm of the star's energy output, or luminosity L, is related to the logarithm of the star's surface temperature T_e. Luminosity is given in units of the sun's luminosity, $L_\odot = 3.86 \times 10^{33}$ ergs per second, and surface temperature is in degrees Kelvin. As time progresses, luminosity and surface temperature of the model star vary along the path in the direction of the arrows. Logarithms in Fig. 1 are to the base 10. Thus, at point 1 in Fig. 1, the 5-$M_\odot$ model emits 580 times as much energy per second as the sun does and is characterized by a surface temperature of about 18,600°K. At point 2, the 5-$M_\odot$ star emits, at a surface temperature of about 15,700°K, 1000 times as much energy per second as the sun does.

The surface temperature of a star is related to its color. The sun, whose surface temperature is roughly 6000°K ($\log T_e = 3.78$), appears yellow. A star with a surface temperature of 4500°K ($\log T_e = 3.65$) would appear red, and a star with a surface temperature greater than 10,000°K ($\log T_e = 4.0$) would appear blue or whitish-blue. Thus, the higher the surface temperature, the bluer the star; the lower the surface temperature, the redder the star. For ease in speaking, it is often convenient to replace a statement concerning surface temperature and luminosity by one involving color and brightness. For example, one may say that, between points 5 and 6 in Fig. 1, the 5-$M_\odot$ model star evolves toward the red and becomes dimmer. Between points 6 and 7, the model star brightens and becomes redder still.

Numbered circles along the path in Fig. 1 denote boundaries of easily distinguished phases. A description of several phases and points is supplied in Fig. 1, and the time spent by the star in these phases is also indicated.

The author is associate professor of physics at Massachusetts Institute of Technology, Cambridge.

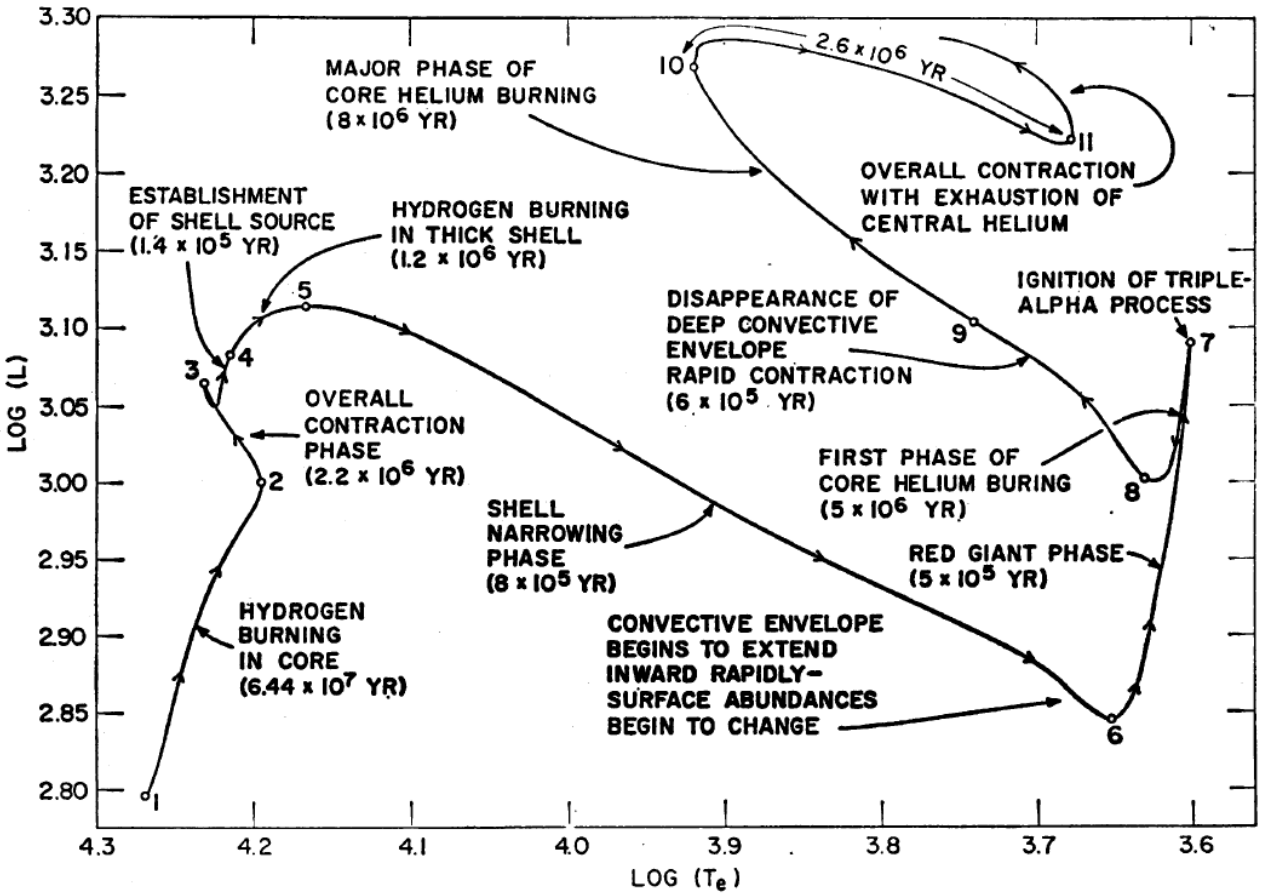

Fig. 1. The evolutionary path of a 5-$M_\odot$ star in the Hertzsprung-Russell diagram. Luminosity L is in units of the sun's luminosity $L_\odot$ ($= 3.86 \times 10^{33}$ ergs per second) and surface temperature T_e is in degrees Kelvin. Traversal times between labeled points are given in years.

THE BIRTHLINE FOR LOW-MASS STARS

STEVEN W. STAHLER
Harvard-Smithsonian Center for Astrophysics, Cambridge, Massachusetts
Received 1983 January 19; accepted 1983 May 4

ABSTRACT

Using the results of protostar theory, I find the locus in the Hertzsprung-Russell diagram where pre–main-sequence stars of subsolar mass should begin their quasi-static contraction phase and first appear as visible objects. This "birthline" is in striking agreement with observations of T Tauri stars, providing a strong confirmation of the fact that these stars are indeed contracting along Hayashi tracks. The assumption that most T Tauri stars first appear along this line forces a recalibration of their ages. This recalibration removes the puzzling dip in present-day star formation seen in age histograms of several cloud complexes. Since the underlying protostar calculation assumes that the parent cloud was only thermally supported prior to its collapse, the observed location of the birthline places severe restrictions on the degree of extrathermal support provided by rotation, magnetic fields, or turbulence. In addition, the hypothesis that the collapse from thermally supported clouds to low-mass stars proceeds through protostellar disks appears untenable, since the disk accretion process almost certainly produces pre–main-sequence stars with radii well below the observed birthline.

Theoretical evolutionary tracks

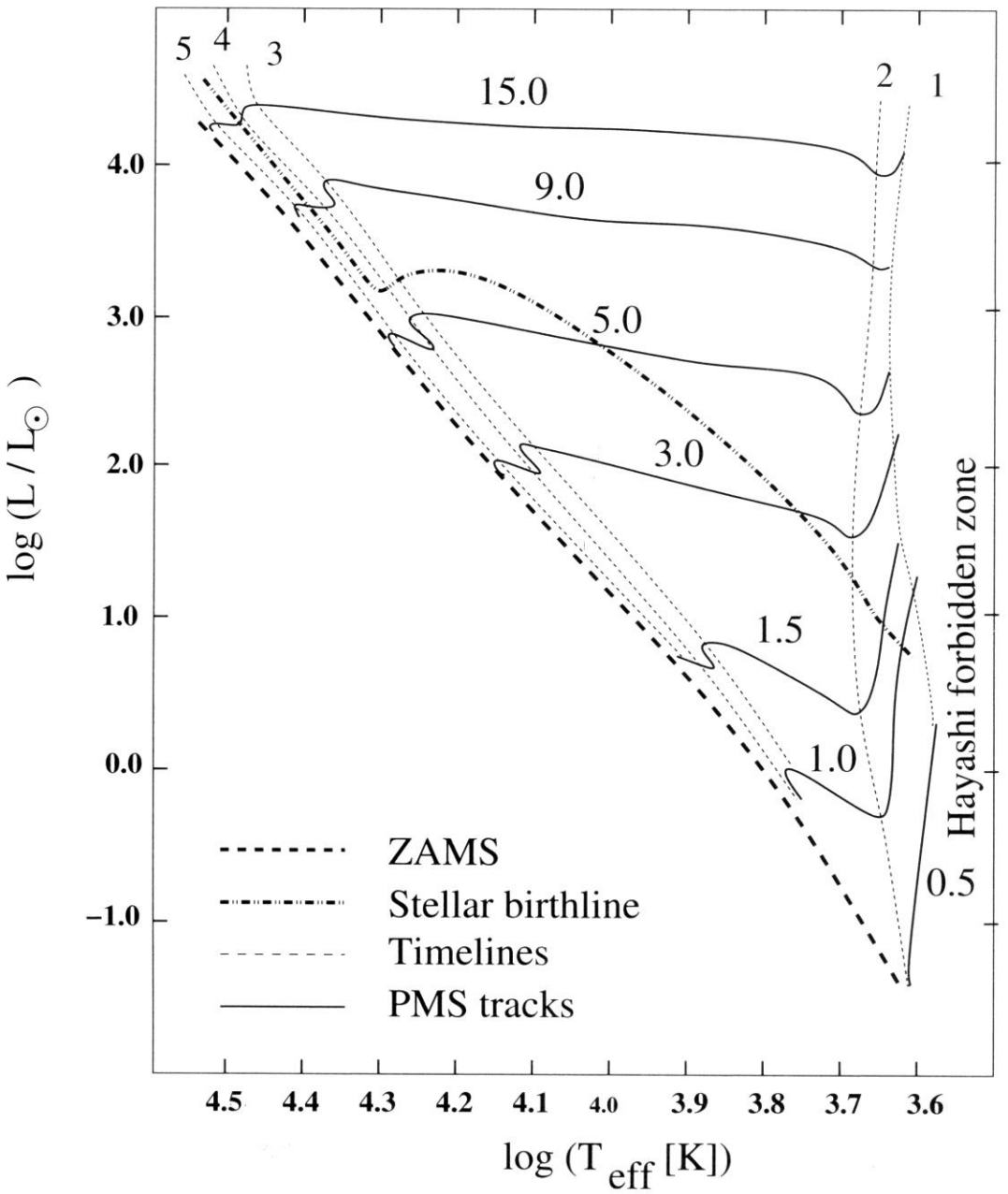

Fig. 6.6. Evolutionary paths in the HR-diagram for stellar masses ranging from 0.5 to 15 $M_\odot$ (solid tracks, adapted from Iben [420]). These paths are marked by thin hatched lines marking time periods labeled 1 to 5. The thick hatched line to the left approximately indicates the location of the ZAMS. The line across the tracks is the stellar birthline approximated from [76] for an accretion rate of $\dot{M}_{acc} = 10^{-5} M_\odot \text{ yr}^{-1}$.

… compared with observations

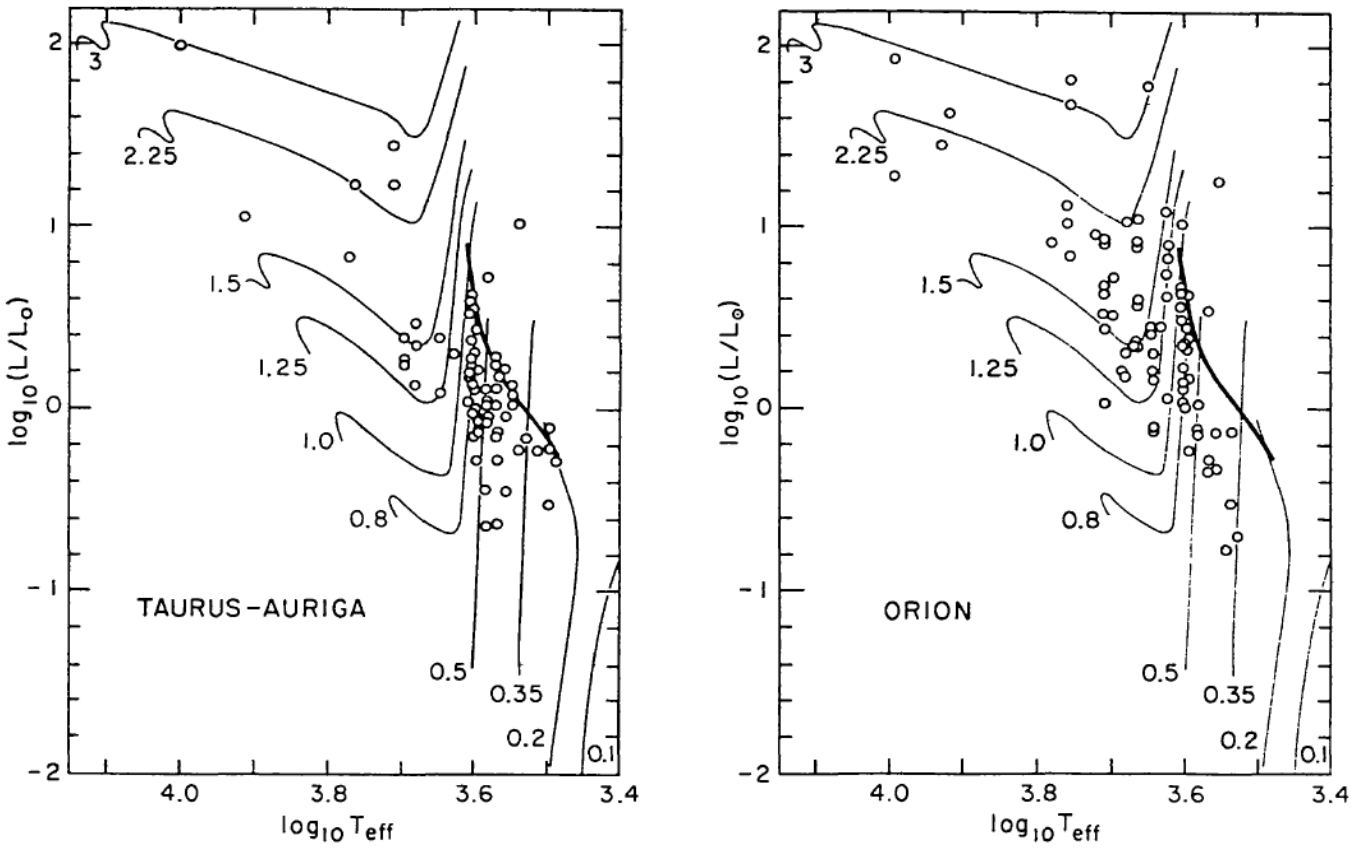

Figure 4 Hertzsprung-Russell diagrams from Cohen & Kuhi (1979) showing theoretical pre-main-sequence contraction tracks and T Tauri stars in the Taurus-Auriga and Orion cloud complexes. The heavy solid curve is the theoretical "birthline" of Stahler (1983).

Observational characteristics of T Tauri stars

TTS: pre-main sequence solar-like stars

- Seen in regions of obscuration
- Spectra types later than F
- Brightness variability (x rays to infrared)

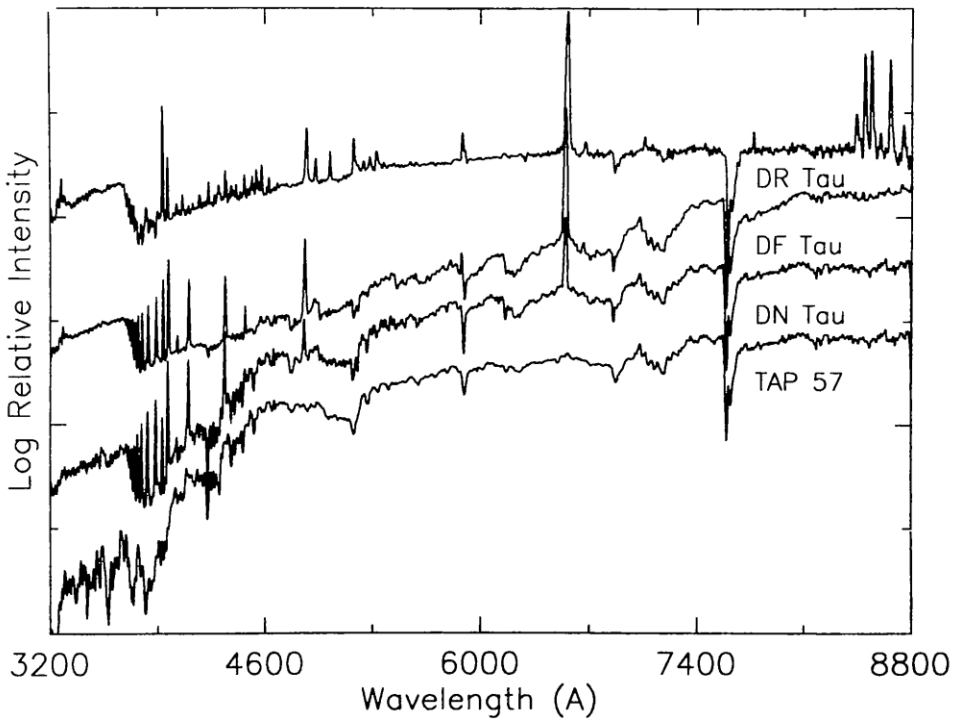

Figure 2 Medium-resolution spectrograms covering the spectral range 3200–8800 Å of four late-K or early-M T Tauri stars, shown in order of increasing emission levels. The relative intensity is displayed in wavelength units.

Strong emission lines in the spectra

Bertout 1989 ARAA

- Lithium absorption λ6708 indicative of youth

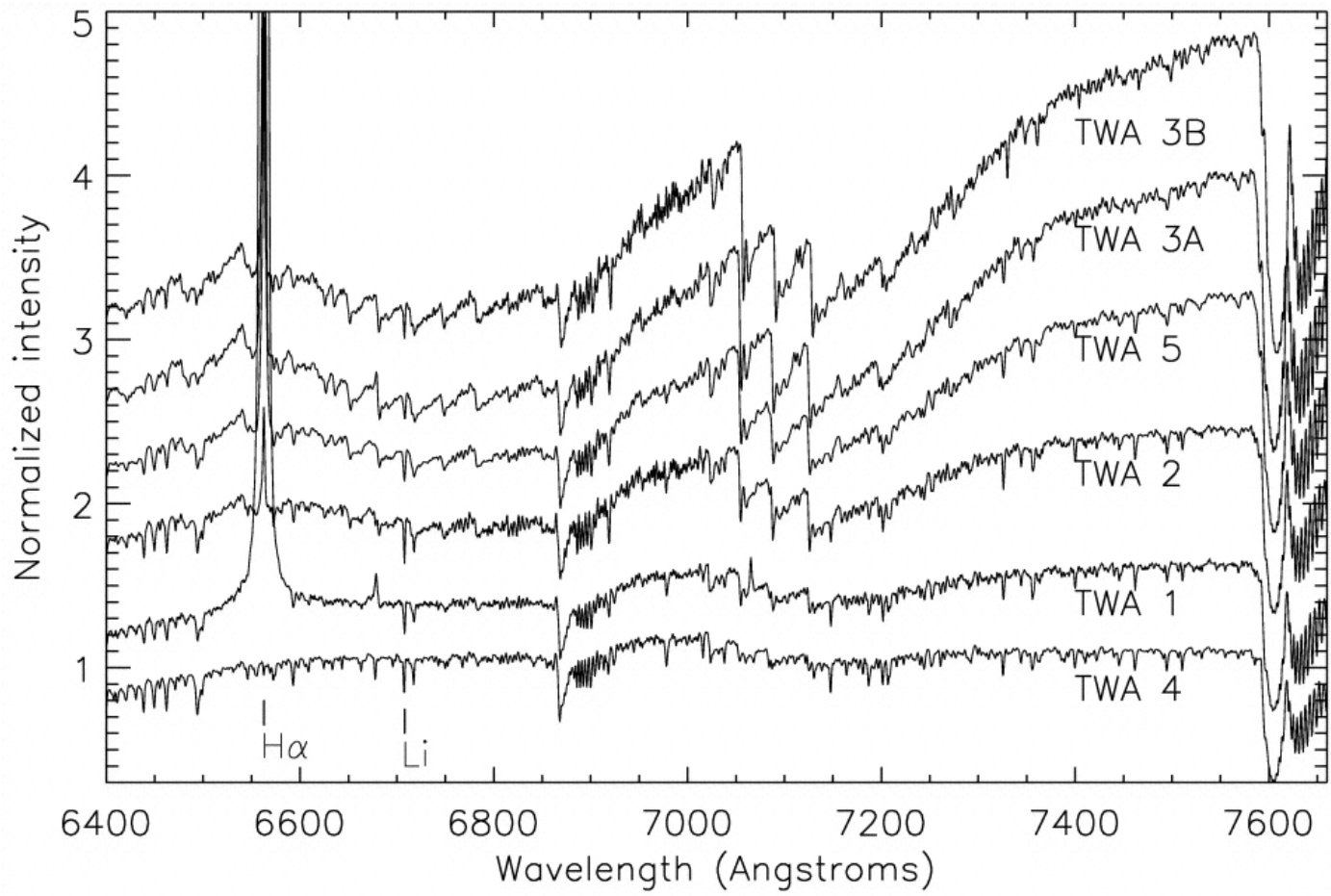

Webb 1999 ApJ, 512, L63 on TW Hya

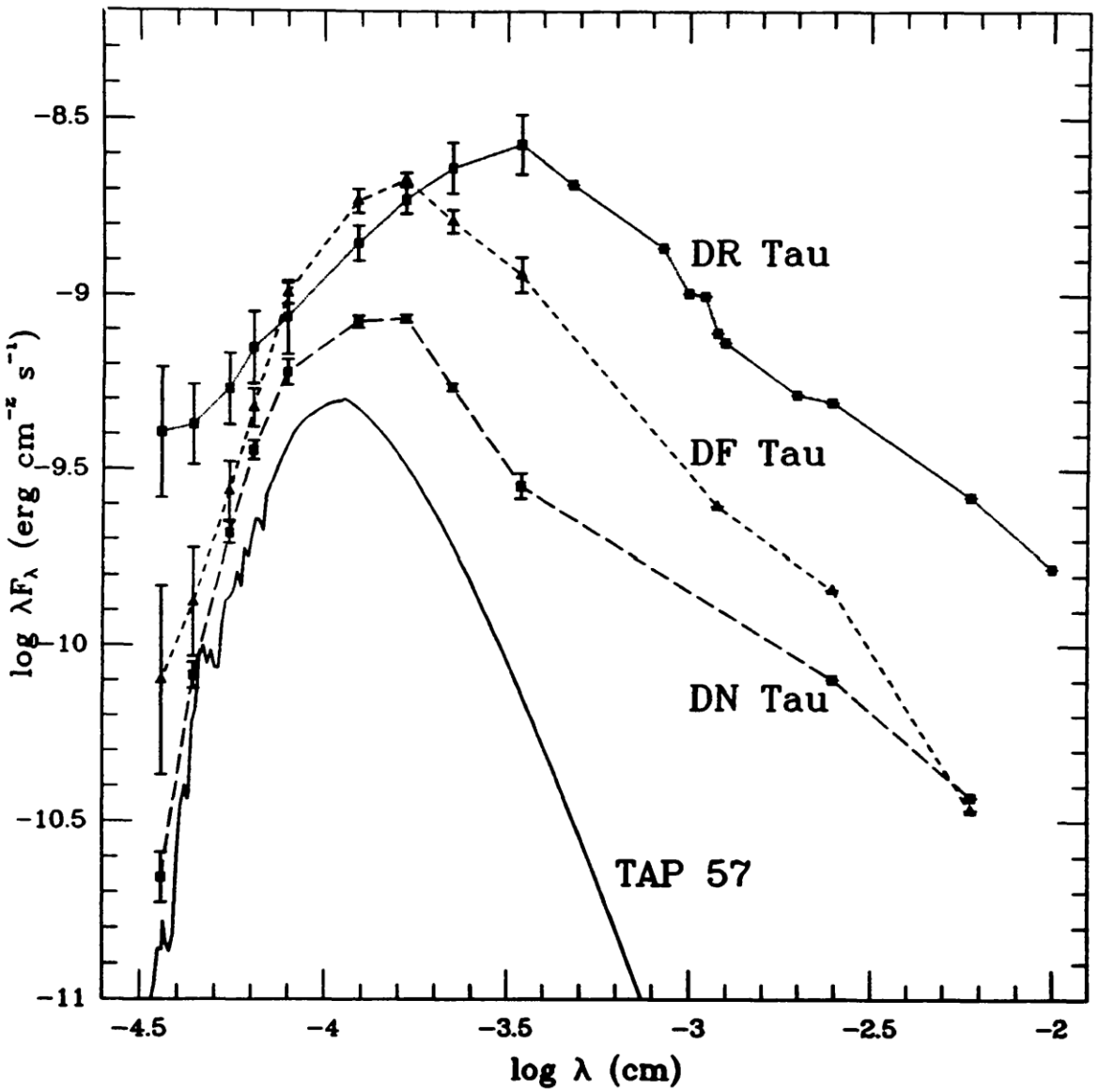

Figure 3 Observed spectral energy distributions from 3600 Å to 100 μm of the stars whose spectra are shown in Figure 2. The energy distribution of the K7V WTTS TAP 57, shown as a solid line, has been displaced downward by 0.3 dex. The filled symbols are simultaneous (for DN Tau and DF Tau) or averaged (for DR Tau) photometric data (cf. Bertout et al. 1988) supplemented by *IRAS* data (Rucinski 1985). When available, observed variability is indicated by error bars. When compared with WTTSs such as TAP 57, CTTSs display prominent ultraviolet and infrared excesses. Excess continuum flux and optical emission-line activity are often correlated.

Excess emission in the IR wavelengths above the stellar photosphere

X-ray emission (and rotation)

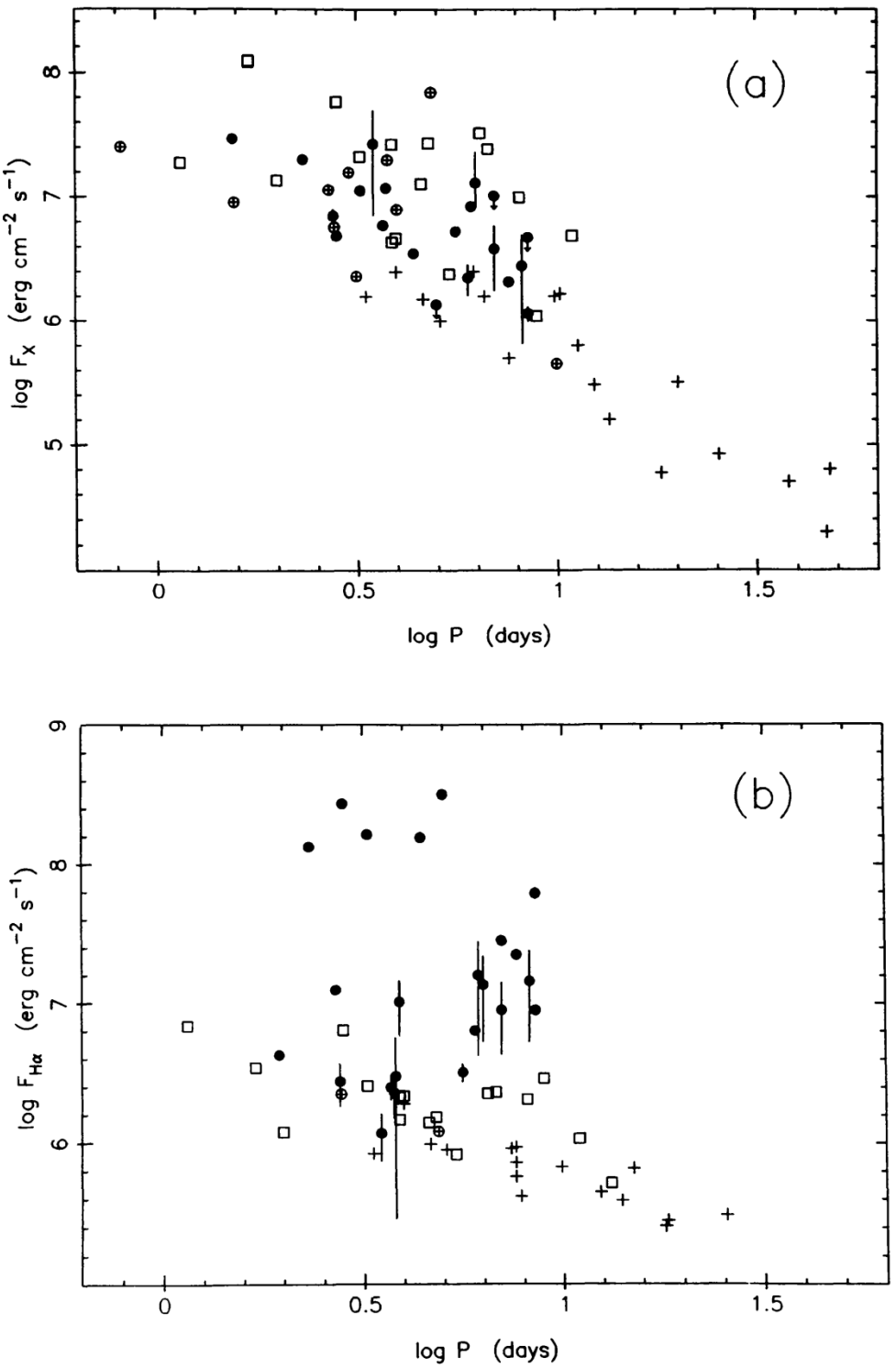

Figure 5 (*a*) Relationship between rotation period and observed X-ray flux for a sample of T Tauri stars and other late-type stars (from Bouvier 1989). T Tauri stars are shown as black dots, and their observed variability (when available) is indicated by a vertical bar. RS CVn stars are displayed as open squares, dKe and dMe stars as open crossed circles, and late-type dwarfs as crosses. The observed correlation between X-ray flux of T Tauri stars and their rotation period closely matches the relationship derived from other late-type stars. (*b*) Relationship between rotation period and observed Hα flux for the same sample of T Tauri stars and other late-type stars as in (*a*) (from Bouvier 1989). While WTTSs follow the same relation as other late-type active stars, CTTSs have much larger Hα fluxes, which are not correlated with the rotation period.

Table 2.1. Space missions relevant for star formation research. The bandpasses are generally given in wavelength units, except for X-ray missions that did not have high spectral resolving power. Here it is more common to specify the range in keV.

Mission	Bandpass spectral range	Mission dates	Major science impact in star-formation research
IUE	UV 1150 – 3299 Å	Jan. 78–Sep. 96	UV spectra of young massive stars, Herbig Ae/Be stars.
EINSTEIN	X-ray 1 – 20 keV	Nov. 78–Apr. 81	Detection of X-rays from low-mass stars.
IRAS	IR 8 – 120 μm	Jan. 83–Nov. 83	All-sky survey, photometry of young stars.
HST	Optical/IR 3000 Å– 3.5 μm	Apr. 90–	High-resolution images of star-forming regions.
ROSAT	X-ray 0.1 – 2.4 keV	Jun. 90–Feb. 99	First X-ray all-sky survey; identifications, distributions and luminosities of young stars.
EUVE	Far-UV 70 – 760 Å	Jun. 92–Jan. 01	All-sky survey catalog, coronal spectra of stars.
ASCA	X-ray 0.3 – 10 keV	Feb. 93–Jul. 00	Hard X-rays from star-forming regions.
ISO	IR/Sub-mm 2.5 – 240 μm	Nov. 95–May 98	High-resolution images and spectra of stellar cores young stars.
SWAS	Sub-mm 487 – 556 μm	Dec. 98–	molecular line emission (i.e., O_2,H_2O,CO) in star-forming regions.
FUSE	Far-UV 905 – 1195 Å	Jun. 99–	Molecular absorption lines in spectra of young stars.
Chandra	X-ray 1.5 – 160 Å	Jul. 99–	High-resolution images and spectroscopy of star-forming regions, line diagnostics.
XMM-Newton	X-ray 6 – 120 Å	Dec. 99–	High-efficiency spectroscopy of young stars.
SST	IR/Sub-mm 3.6 – 160 μm	Aug. 03–	Imaging and spectroscopy of star-forming regions with high precision.
SOFIA	2.2 – 26 μm	2004–	Permanent IR observatory flying at 13 km above ground.
JWST	Optical/IR	Approx. 2011	Images beyond HST.
Herschel	Far-IR/Sub-mm	Feb. 2007	Star formation in galaxies interstellar medium.
GAIA	Optical	Mar. 2010	3-D mapping of the Galaxy.